1 **TITLE:**

2 ***In vivo* KRAS G12D/V degradation mediated by CANDDY using a modified**

3 **proteasome inhibitor**

4

5 **AUTHORS/AFFILIATIONS:**

6 **Satoshi Imanishi[1,#], Lijuan Huang[1,#], Shoko Itakura[2], Masamichi Ishizaka[1,3],**

7 **Yoichi Iwasaki[1,3], Tomohiro Yamaguchi[1,3], and Etsuko Miyamoto-Sato[1,2,3*]**

8 [1] Laboratory of Miyamoto-Sato Molecular Medical Sciences, Research Institute for

9 Science & Technology, Tokyo University of Science, 2641 Yamazaki, Noda, Chiba

10 278-0022, Japan

11 [2]Graduate School of Biological Sciences, Tokyo University of Science, 2641 Yamazaki,

12 Noda, Chiba 278-0022, Japan

13 [3]R & D Department, FuturedMe Inc., 2641 Yamazaki, Noda, Chiba 278-0022, Japan

14 [#]These authors contributed equally to this work.

15 [*] Correspondence: nekoneko@rs.tus.ac.jp

16

Abstract

"Undruggable" proteins, such as RAS proteins, remain problematic despite efforts to discover inhibitors against them. KRAS mutants are prevalent in human cancers. Recently, the KRAS G12C inhibitor have been clinically approved, but inhibitors for KRAS G12D/V are still under development. Here, we described the development of a novel chemical knockdown strategy, termed CANDDY (Chemical knockdown with Affinity aNd Degradation DYnamics). This strategy involves a CANDDY tag modified from a proteasome inhibitor inducing direct proteasomal degradation. We constructed TUS-007 as a multispecific small molecule tethered from a KRAS interactor and CANDDY tag to target KRAS G12D/V. We confirmed that the degradation by TUS-007 was independent of target ubiquitination. This allows to solve a laborious design of matchmaker in the current ubiquitination-dependent proteolysis technology. And TUS-007 successfully suppressed tumors due to *in vivo* degradation of KRAS G12D/V. The CANDDY technology could represent a simple and rational strategy to degrade currently "undruggable" proteins.

Introduction

The majority (75%) of disease-causing proteins are "undruggable" (i.e., difficult to inhibit with small molecules). This difficulty reflects in the presence of smooth surfaces and lack of deep pockets, including proteins associated with cancer drivers and many interfaces for protein-protein interaction (PPI) (1, 2, 3). RAS family members (e.g., KRAS, HRAS, and NRAS) are most challenging to inhibit by small molecules (1, 4, 5, 6, 7). Mutations of KRAS, especially G12C, G12D, and G12V, are frequent in human cancers (7). The RAS protein activities depend on nucleotide loading in their GTP-binding pockets. The inhibition of this pocket has been attempted for nearly 40 years. However, progress has been hindered by the exceptionally high affinity between GTP and RAS proteins (1, 4, 8). While the inhibitor targeting KRAS G12C have been clinically approved recently (6, 9), inhibitors for KRAS G12D/V, which addresses greater clinical need, are still remained under development. These are important targets found in 95% of pancreatic cancers and 64% of colon cancers (7, 8). Inhibitors of the PPI between RAS and Son of Sevenless 1 (SOS1) (RAS-SOS inhibitor) have been investigated. Inhibitors that directly bind to RAS are not effective owing to their low

48 affinity (5). Thus, the current inhibition technologies are not enough to be effective for
49 undruggable proteins.
50 Pharmaceutical research on undruggable proteins, such as RAS, focuses on novel
51 modalities instead of inhibition (10, 11, 12). Proteolysis technologies, using
52 matchmakers between the target and E3 ligase or other ubiquitination related proteins
53 such as molecular chaperons for inducing target degradations, are expected to be
54 effective against undruggable proteins (13, 14, 15, 16, 17). However, matchmaker
55 design has been hampered by the dependency on target ubiquitination (16). It is difficult
56 to select a suitable E3 ligase for a target of interest because of limited knowledge about
57 the mechanism underlying substrate recognition by E3 ligases. Even if the target has an
58 established corresponding E3 ligase, there may be no available ligand for the E3 ligase.
59 Moreover, target ubiquitination may not always induce proteolysis, as in the case of
60 RAS, in which ubiquitination also regulates protein localization and activation (18).
61 Despite such difficulties, an effective inhibitor (9) was used recently for a proteolysis
62 inducer of KRAS G12C (19). However, no proteolysis inducer for KRAS G12D/V has
63 been reported. Current proteolysis technologies that depend on ubiquitination have

64 limited efficacy for undruggable targets (14). Therefore, to modulate diverse

65 undruggable targets, the difficulties in matchmaking should be eliminated (13).

66 Here, we report successful KRAS G12D/V degradation, mediated by a novel tool

67 named CANDDY (Chemical knockdown with Affinity aNd Degradation DYnamics).

68 This innovative approach induces direct proteasomal degradation (i.e., chemical

69 knockdown) of the target using a CANDDY tag derived from a proteasome inhibitor

70 that lacks the site for inhibitory activity (inhibitor site). By CANDDY technology,

71 chemical knockdown occurs without ubiquitination, so it can bypass the difficulties of

72 designing a matchmaker in current proteolysis techniques (13). Using an inefficient

73 target inhibitor, RAS/SOS inhibitor (5), we designed and synthesized a CANDDY

74 molecule called TUS-007 for KRAS G12D/V. We demonstrated KRAS G12D/V

75 chemical knockdown mediated by TUS-007 in cell-free, *in vitro*, and *in vivo* assays,

76 and *in vivo* tumor suppression.

77

78 **Results**

79 **A CANDDY molecule for targeting KRAS G12D/V proteins**

80 CANDDY molecules are bispecific molecules constructed from two modules;
81 a target interactor, which enables specific binding to the target, and a CANDDY tag,
82 which induces proteasomal degradation (Fig. 1a). The CANDDY tag is essential in
83 CANDDY technology and is a derivative lacking the inhibitor site of MLN2238 (MLN)
84 (20), a clinical proteasome inhibitor (Fig. 1b and Text S1.). To design TUS-007, we
85 employed a RAS-SOS inhibitor (5) (shown in Fig. 1c) which directly binds to KRAS
86 G12D, KRAS G12V, and wild-types of KRAS and HRAS as the target interactor
87 module. Since the binding to wild-type NRAS have not been reported, it was expected
88 to avoid the severe toxicity observed in a pan-RAS inhibitor (21). RAS-SOS inhibitor
89 was conjugated to the CANDDY tag using a NH_2 linker (Fig. 1c and Text S1.).
90 To compare the target binding of TUS-007 with that of the RAS-SOS
91 inhibitor, we performed a thermal shift assay. Unexpectedly, KRAS G12D/V proteins
92 incubated with TUS-007 were more resistant against heat treatment than those
93 incubated with RAS-SOS inhibitor (Fig. S1a). Alternatively, in a fluorescence-based
94 thermal shift assay, the T_m value of KRAS G12D incubated with TUS-007 was higher
95 than that of KRAS G12D incubated with RAS-SOS inhibitor (Fig. 1d and Fig. S1b).

96 These results suggest the higher affinity of TUS-007 to KRAS compared to RAS-SOS

97 inhibitor. In addition, we confirmed that TUS-007 had no inhibitory activity against the

98 catalytic β-subunits of proteasome (Fig. S2). This demonstrated that the CANDDY tag,

99 modified from a proteasome inhibitor, hardly inhibit proteasome activity.

100

101 **Chemical knockdown of KRAS G12D/V free from ubiquitination by TUS-007**

102 We attempted a chemical knockdown of KRAS G12D in the presence of 26S

103 proteasomes and in the absence of any ubiquitination related proteins in a cell-free

104 assay. Successful degradation was performed with 50% degradation concentration

105 (DC50) at 4 μM (Fig. 1e). The chemical knockdown mediated by TUS-007 was

106 counteracted by the presence of MLN (Fig. 1f). Additionally, RAS-SOS-NH_2 (a

107 synthetic intermediate without CANDDY tag, Fig. 1c) as a degradation-incompetent

108 control failed to induce the chemical knockdown (Fig. 1f), demonstrating CANDDY tag

109 is essential to induce the chemical knockdown. Although RAS-SOS inhibitor showed

110 80% inhibition of RAS-SOS PPI at 1 mM (5), DC80 of TUS-007 for KRAS G12D was

111 estimated as 16 μM (Fig. 1e). It implied that the conjugation with CANDDY tag

112 drastically improved the usefulness of RAS-SOS inhibitor. We also confirmed chemical

113 knockdown of KRAS G12V by TUS-007 in a cell-free assay in the absence of any

114 ubiquitination related proteins (Fig. S3). Furthermore, to obtain additional evidence of

115 degradation independent of ubiquitination, we co-treated HeLa cells expressing GFP-

116 KRAS G12D and DsRed with TUS-007 and MLN, E1 inhibitor (NAEi) or HSP70

117 inhibitor (VER-155008) (Fig. 2a). MLN counteracted the lowering of GFP signal

118 induced by TUS-007 treatment, but NAEi or VER-155008 did not. These results

119 demonstrated that chemical knockdown induced by TUS-007 was depend on

120 proteasome and independent of ubiquitination processes.

121

122 **TUS-007 induced targets-selective chemical knockdown *in vitro***

123 Using an *in vitro* assay, we then evaluated the chemical knockdown and

124 investigated the selectivity of TUS-007. We utilized RAS-less mouse embryonic

125 fibroblasts (MEFs) expressing human KRAS G12D, G12V, or G12C. These MEFs do

126 not proliferate in the absence of RAS (22). Immunoblotting analysis revealed that TUS-

127 007 induced the chemical knockdown of KRAS G12D/V, but not G12C, in RAS-less

128 MEFs (Fig. 2b). TUS-007 reduced the viability of RAS-less MEFs expressing KRAS
129 G12D/V but did not affect the viability of the cells expressing KRAS G12C (Fig. 2c),
130 confirming the selectivity of TUS-007 for KRAS G12D/V. We also assessed the
131 selectivity of TUS-007 for the human RAS family, including wild-type KRAS, HRAS,
132 and NRAS. TUS-007 did not affect the NRAS protein levels or the viability of RAS-
133 less MEFs expressing NRAS but affected KRAS or HRAS levels and the viability of
134 RAS-less MEFs expressing KRAS or HRAS (Fig. S4a and b). This result is consistent
135 with the previously reported data on the selectivity of the RAS-SOS inhibitor (5).
136 Therefore, it is expected not to induce intolerable toxicity previously observed with a
137 pan-RAS inhibitor *in vivo* (21) since TUS-007 is not a pan-RAS degrader. Furthermore,
138 the viability of RAS-less MEFs expressing KRAS G12C maintained even at 100 μM
139 TUS-007 (Fig. 2b and c), indicating that TUS-007 might have no remarkable off-target
140 toxicity in cell even at high concentrations. These results demonstrated the correlation
141 between the degradation of targets and the viability of cells by the concentrations of
142 TUS-007 without non-specific cytotoxic effect (Fig. 2b and c).
143

144 **The effects of TUS-007 on KRAS G12V-driven colon cancer**

145 Approximately 64% of human colon cancers reportedly express KRAS

146 mutants. KRAS G12V is found in nearly half of the patients and is correlated with poor

147 prognosis (8). Therefore, we investigated whether TUS-007 can suppress the growth of

148 human KRAS G12V-driven colon cancer cells. We conducted an experiment with the

149 SW620-Luc KRAS G12V homozygous human colon cancer cell line (23). TUS-007

150 induced chemical knockdown of KRAS (Fig. 3a), accompanied by an increase in the

151 annexin V-positive fraction in SW620-Luc cells (Fig. 3b and Fig. S5). However, RAS-

152 SOS-NH_2 and cetuximab did not induce apoptosis (Fig. 3b and Fig. S5). In contrast,

153 treatment with TUS-007 did not result in significant changes in the annexin V-positive

154 fraction in HT29-Luc RAS-independent colon cancer cells (Fig. 3c and Fig. S6).

155 Alternatively, the apoptosis induction in SW620-Luc cells was confirmed by caspase

156 3/7 activation (Fig. 3d). Importantly, TUS-007 induced the apoptosis in SW620-Luc

157 cells at the same concentration at which the chemical knockdown of KRAS was

158 significant (Fig. 3a, b and Fig. S7). These findings indicated that TUS-007 selectively

159 induces apoptosis in SW620-Luc cells by chemical knockdown of KRAS G12V *in*

160 *vitro*.

161 Next, to assess the effectiveness of TUS-007 *in vivo*, we transplanted SW620-

162 Luc cells subcutaneously in immunodeficient mice. TUS-007 or cetuximab was

163 administered to the xenograft mice by intraperitoneal (i.p.) injection. TUS-007

164 significantly attenuated tumor progression (Fig. 3e, f and Fig. S8a) and induced KRAS

165 G12V chemical knockdown in tumors (Fig. S8b). The body weights of the mice were

166 not affected by TUS-007 treatment (Fig. S8c). These results suggested that TUS-007 is

167 effective *in vivo* against KRAS G12V-driven tumors.

168

169 **The effects of TUS-007 on KRAS G12D-driven pancreatic cancer**

170 Approximately 95% of pancreatic cancers harbor KRAS mutations, and the

171 G12D mutation is particularly prevalent and strongly correlated with poor prognosis (8).

172 Therefore, we examined the effects of TUS-007 in human pancreatic cancer cell lines.

173 As expected, TUS-007 degraded the KRAS protein (Fig. 4a) and induced apoptosis

174 (Fig. 4b) in SW1990 KRAS G12D-driven pancreatic cancer cells (24). The apoptosis

175 induction in SW1990 cells was approximately correlated with concentrations of

176 chemical knockdown of KRAS (Fig. 4a and b). The correlation between the

177 concentration of apoptosis induction and degradation induction was further confirmed

178 (Fig. S9). In addition, apoptosis was induced with caspase 3/7 activation in SW1990

179 cells (Fig. 4c), which was counteracted by a proteasome inhibitor MLN but not by a

180 ubiquitination inhibitor NAEi (Fig. 4d). Therefore, it suggested that TUS-007 induced

181 apoptosis owing to target degradation independent of ubiquitination.

182 In mice with SW1990 cells implanted subcutaneously, the oral (per os; p.o.)

183 administration of TUS-007 significantly suppressed the tumor growth (Fig. 4e) and

184 reduced tumor weight (Fig. S10a). The i.p. injection of TUS-007 also suppressed

185 subcutaneously implanted tumor growth in mice (Fig. S10b). Both p.o. (Fig. 4f) and i.p.

186 (Fig. S10c) administrations showed no change in body weight. Here, we examined the

187 chemical knockdown of KRAS, HRAS and NRAS with TUS-007 in pancreas from the

188 identical mice used in Fig. 4e and f. In accordant with the results in RAS-less MEFs,

189 TUS-007 induced the degradation of KRAS and HRAS but not NRAS (Fig. S11). Thus,

190 there was no sign of toxicity such as body weight losses in contrast to a pan-RAS

191 inhibitor (21).

192 Moreover, extracellular signal-regulate kinase (ERK) and protein kinase B

193 (AKT) phosphorylation were decreased in tumor by both p.o. and i.p. administrations

194 (Fig. S12a and b), indicating that both RAS-mitogen-activation protein (RAS-MAP)

195 and RAS- phosphoinositide 3-kinase (RAS-PI3K) signaling were inhibited. It is

196 difficult for inhibitors to inhibit both RAS-MAP and RAS-PI3K signaling, even using a

197 clinically effective KRAS G12C inhibitor (6). Thus, the chemical knockdown of KRAS

198 by CANDDY might offer a clinical benefit. Taken together, these results indicated that

199 TUS-007 exerted *in vivo* antitumor activity *via* the chemical knockdown of KRAS

200 G12D/V and suppression of KRAS signaling.

201

202 **TUS-007 exerted anti-tumor activity even in orthotopic xenograft model mice**

203 SW1990-Luc cells were transplanted directly into the pancreas of mice as an

204 orthotopic xenograft model. The mice were subsequently treated p.o. with TUS-007.

205 Remarkably, *in vivo* imaging revealed reductions in tumor growth (Fig. 5a, b and Fig.

206 S13a) and tumor weight (Fig. S13b). Results from immunohistochemical analysis (Fig.
207 5c left panels and Fig. S13c left bar graph) and immunoblotting (Fig. 5d) confirmed the
208 chemical knockdown of KRAS G12D in the tumor tissues of mice treated with TUS-
209 007. Furthermore, higher concentrations of positive cells were observed in the terminal
210 deoxynucleotidyl transferase dUTP nick-end labeling (TUNEL) assay in the tumor
211 tissues of TUS-007-treated mice, implying the induction of apoptosis in the TUS-007-
212 treated tumors (Fig. 5c right panels and Fig. S13c right bar graph). The body weights of
213 the orthotopic xenograft model mice were not affected by TUS-007 (Fig. S13d).
214 Overall, these results demonstrated that oral treatment with TUS-007 induces KRAS
215 G12D chemical knockdown and suppresses pancreatic tumor growth without the sign of
216 weight loss and significant toxicity in the orthotopic xenograft model.
217 We examined the *in vivo* concentrations of TUS-007. When an i.p dose of 80
218 mg/kg TUS-007 was administered to healthy mice, a concentration (45 ng/mg,
219 equivalent to 53 μM) of TUS-007 was observed in the pancreas (Table S1.). This TUS-
220 007 concentration *in vivo* agreed with the concentration at which chemical knockdown
221 and apoptotic indicators were observed in SW1990 cells *in vitro* (Fig. 4a-c). Therefore,

222 these results suggest that there is no contradiction between our *in vivo* and *in vitro*

223 results.

224 Finally, to examine TUS-007 toxicity in detail, the general, histological,

225 hematological and biochemical examinations using mice were performed. The p.o.

226 treatment of TUS-007 at 80 mg/kg for continuous 5 days did not cause any toxic effect

227 in body weight, organ weight, histology of organs, hematology and blood biochemistry

228 at 2 weeks after the last treatment (Table S2-S6.). Thus, oral treatment with TUS-007

229 did not show sever toxicity.

230

231 **CANDDY applied to another undruggable target**

232 To evaluate the versatility of CANDDY approach, we designed a CANDDY

233 molecule targeting MDM2 (MDM2-CANDDY), a negative regulator of P53, using a

234 P53-MDM2 PPI inhibitor with a weak potency (25) as an interactor module of a

235 CANDDY molecule (Fig. S14a and Text S1.). MDM2-CANDDY successfully induced

236 the chemical knockdown of MDM2 in HCT-116 human colon cancer cells (Fig. S14b).

237 P53-MDM2 PPI is still well-recognized “undruggable” target (26). This result

238 suggested the potential versatility of CANDDY to target other undruggable proteins.

239

240 **Discussion**

241 We provided the proof of concept that CANDDY tag enabled to induce

242 proteasomal degradation through ubiquitination-independent process (Fig. 1f and Fig.

243 2a) in this report. Considering the proteasome enable to degrade any targets, the

244 CANDDY tag modified from a proteasome inhibitor (Fig. 1b) can eliminate the

245 difficulties of matchmaking of targets and specific ubiquitination related proteins such

246 as E3 ligases in current protein degradation (13, 14). Thus, CANDDY technology could

247 provide a simple and rational approach to induce the chemical knockdown of currently

248 undruggable targets because of the CANDDY tag independent of ubiquitination.

249 Expectedly, we confirmed the correlations between degradation of KRAS

250 G12D and V and apoptosis in pancreatic and colon cancer cells, respectively (Fig. 3a, b,

251 Fig. 4a-d, Fig. S7 and S9), and *in vivo* (Fig. 5c and Fig. S13c). Both *in vitro* and *in vivo*,

252 TUS-007 achieved efficacy mediated by moderate degradations of KRAS G12D/V. A

253 previous study showed that the moderate decrease of KRAS protein is enough to inhibit
254 tumor growth *via* more strong inhibition of downstream signal (12) as well as we
255 showed (Fig. S12). Thus, *in vitro* and *in vivo* results could be reasonable. Importantly,
256 the concentration of TUS-007 in pancreas agreed with the effective concentration *in*
257 *vitro* (Table S1.), demonstrating the consistency between our *in vivo* and *in vitro* results.
258 On the other hand, the requirement of high concentrations generally raises concerns
259 about toxicity. However, TUS-007 did not show non-specific cytotoxicity *in vitro* even
260 at high concentration (Fig. 2c) and no sign of body weight losses was observed in TUS-
261 007 treated mice (Fig. 4f, Fig. S8c, S10c and S13d) in contrast to a pan-RAS inhibitor
262 (21). These results suggest that TUS-007 induced *in vivo* degradation of KRAS
263 G12D/V resulting in suppression of colon and pancreatic tumors without no significant
264 toxicity even at high concentrations.

265 No effective drug to inhibit or degrade KRAS G12D/V has been reported yet.
266 Also, the proteolysis field does not still have enough evidence that can target and
267 degrade tough and valuable undruggable proteins (14). Of note, in spite of a poor
268 inhibitor was employed as interactor, TUS-007 induced chemical knockdown of KRAS

269 G12D/V *in vivo*, resulting in suppression of a pancreatic tumor even in the orthotopic

270 xenograft model with oral administrations (Fig. 5). In addition, another weak inhibitor

271 of PPI, P53-MDM2 PPI inhibitor (25) (Fig. S14), was useful as the interactor of

272 CANDDY molecules. Thus, CANDDY technology could be expectedly applied to

273 tough and valuable undruggable targets still remaining with no effective inhibitors. In

274 the future, CANDDY has the potential to overcome the current limitations of

275 proteolysis and to expand the application scope of degraders for molecular targeting

276 therapy of aggressive and deadly diseases caused by undruggable targets.

277

References

1. Khan, I., Rhett, J. M. & O'Bryan, J. P. Therapeutic targeting of RAS: New Hope for drugging the "undruggable". *Biochim. Biophys. Acta Mol. Cell Res.* **1867**, 118570 (2020).
2. Fujimori, S., et al. Next-generation sequencing coupled with a cell-free display technology for high-throughput production of reliable interactome data. *Sci. Rep.* **2,** 691 (2012).
3. Scott, D. E., Bayly, A. R., Abell, C. & Skidmore, J. Small molecules, big targets: Drug discovery faces the protein-protein interaction challenge. *Nat. Rev. Drug Discov.* **15,** 533–550 (2016).
4. Stephen, A. G., Esposito, D., Bagni, R. K. & McCormick, F. Dragging Ras back in the ring. *Cancer Cell* **25,** 272–281 (2014).
5. Sun, Q., et al. Discovery of small molecules that bind to K-Ras and inhibit Sos-mediated activation. *Angew. Chem. Int. Ed.* **51,** 6140–6143 (2012).
6. Canon, J., et al. The clinical KRAS(G12C) inhibitor AMG 510 drives anti-tumour immunity. *Nature* **575,** 217–223 (2019).

295 7. Hobbs, G. A., Der, C. J. & Rossman, K. L. RAS isoforms and mutations in cancer at
296 a glance. *J. Cell Sci.* **129,** 1287–1292 (2016).
297 8. Haigis, K. M. KRAS alleles: The devil is in the detail. *Trends Cancer* **3,** 686–697
298 (2017).
299 9. Sheridan, C. Grail of RAS cancer drugs within reach. *Nat. Biotechnol.* **38,** 6–8
300 (2020).
301 10. Shin, S. M., et al. Antibody targeting intracellular oncogenic Ras mutants exerts
302 anti-tumour effects after systemic administration. *Nat. Commun.* **8,** 15090 (2017).
303 11. Yin, W. & Rogge, M. Targeting RNA: A transformative therapeutic strategy. *Clin.*
304 *Transl. Sci.* **12,** 98–112 (2019).
305 12. Ross, S. J., et al. Targeting KRAS-dependent tumors with AZD4785, a high-affinity
306 therapeutic antisense oligonucleotide inhibitor of KRAS. *Sci. Transl. Med.* **9,** pii:
307 eaal5253. doi: 10.1126/scitranslmed.aal5253 (2017).
308 13. Deshaies, R. J. Multispecific drugs herald a new era of biopharmaceutical
309 innovation. *Nature* **580,** 329–338 (2020).

310 14. Scudellari, M. Protein-slaying drugs could be the next blockbuster therapies. *Nature*
311 **567,** 298–300 (2019).
312 15. Cromm, P. M. & Crews, C. M. Targeted protein degradation: From chemical
313 biology to drug discovery. *Cell Chem. Biol.* **24,** 1181–1190 (2017).
314 16. Pettersson, M. & Crews, C. M. PROteolysis TArgeting Chimeras (PROTACs) -
315 Past, present and future. *Drug Discov. Today Technol.* **31,** 15–27 (2019).
316 17. Churcher, I. Protac-induced protein degradation in drug discovery: Breaking the
317 rules or just making new ones? *J. Med. Chem.* **61,** 444–452 (2018).
318 18. Dohlman, H. G. & Campbell, S. L. Regulation of large and small G proteins by
319 ubiquitination. *J. Biol. Chem.* **294,** 18613–18623 (2019).
320 19. Bond, M. J., et al. Targeted degradation of oncogenic KRASG12C by VHL-
321 recruiting PROTACs. *ACS Cent. Sci.* **6**, 1367–1375 (2020).
322 20. Kisselev, A. F., van der Linden, W. A. & Overkleeft, H. S. Proteasome inhibitors:
323 An expanding army attacking a unique target. *Chem. Biol.* **19,** 99–115 (2012).
324 21. Welsch, M. E., et al. Multivalent small-molecule pan-RAS inhibitors. *Cell* **168,**
325 878–889.e29 (2017).

326 22. Drosten, M., et al. Genetic analysis of Ras signaling pathways in cell proliferation,
327 migration and survival. *EMBO J.* **29,** 1091–1104 (2010).
328 23. Ahmed, D., et al. Epigenetic and genetic features of 24 colon cancer cell lines.
329 *Oncogenesis* **2,** e71 (2013).
330 24. Jansen, J. M., et al. Inhibition of prenylated KRAS in a lipid environment. *PLOS*
331 *ONE* **12,** e0174706 (2017).
332 25. Kumar, S. K., et al. Design, synthesis, and evaluation of novel boronic-Chalcone
333 derivatives as antitumor agents. *J. Med. Chem.* **46**, 2813–2815 (2003).
334 26. Shangary, S. & Wang, S. Targeting the MDM2-p53 Interaction for Cancer Therapy.
335 *Clin. Cancer. Res.* **14,** 5318–5324 (2008).
336 27. Scott, D. E., Bin, Y. & Charlene F. Proteolysis targeting chimeras (PROTACs) in
337 'beyond rule-of-five' chemical space: Recent progress and future challenges, *Bioorg*
338 *Med Chem Lett*, **29**, 1555–1564 (2019).
339

340 **Data availability**

341 Source data are provided for all experiments. Other data that support the

342 findings of this study are available from the corresponding author, upon reasonable

343 request.

344

345 **Acknowledgments**

346 We thank Masaaki Ozawa, Mai Hasegawa, Takuya Yogi, Mizuki Kanazawa, and

347 Sachi Tsuji for help with the *in vitro* studies, Yuri Sato for help with the *in vivo* studies,

348 Megumi Tsukamoto and Megumi Saito for help with both *in vitro* and *in vivo* studies.

349 We thank the NCI RAS initiative for providing the RAS-less MEFs used in this work,

350 the Uchiro Laboratory for performing the high-resolution mass spectrometry analysis at

351 the Research Equipment Center (Tokyo University of Science (TUS), Japan), the Gunji

352 Laboratory (TUS) for the use of their high-performance liquid chromatography

353 instruments, the Iwakura and Abe Laboratories in the animal facility of the Research

354 Institute for Biomedical Sciences (TUS) for maintaining the mice, Fumito Ishizuka and

355 Naoki Takeda (NARD Institute, Ltd.) for contributions to the chemical synthesis, and

Hiroyuki Ohashi for the helpful suggestions. This work was financially supported by the Program for Creating STart-ups from Advanced Research and Technology (START Program: 962238), and the joint research with FuturedMe Inc.

Author contributions

S. Im., L. H., S. It., and E. M. S. designed the study. S. Im., L. H., S. It., M. I. and T. Y. performed the *in vitro* and *in vivo* experiments. Y. I. performed chemical analyses. E. M. S. supervised the study. All authors discussed the study and approved the submitted manuscript.

Competing interests

The authors declare no competing interests.

Supplementary information, including Materials and methods, Text S1, Fig. S1-14 and Table S1-6, is available in the online version of the paper.

373 **Figure legends**

374

375 **Fig. 1. RAS chemical knockdown *in vitro*.**

376 **a,** Principle of the CANDDY technology. Each CANDDY molecule includes a target

377 interactor (burgundy hexagon) and a CANDDY tag (yellow oval). The target protein is

378 bound by the CANDDY molecule *via* the target interactor and is directly degraded by

379 proteasome via the CANDDY tag. **b,** The CANDDY tag was synthesized by chemically

380 inactivating the inhibitor site of MLM2238 (MLN). **c,** Structures of the RAS-SOS

381 inhibitor (ref. 5), RAS-SOS-NH_2, and TUS-007. **d,** KRAS G12D was mixed with

382 DMSO, RAS-SOS inhibitor (4 μM) or TUS-007 (4 μM) and incubated under heating

383 from 25 °C to 99 °C. The denature of KRAS G12D was monitored by the fluorescence.

384 The typical curve of each group was shown. **e,** The correlation between relative amount

385 of KRAS G12D and concentration of TUS-007 were approximated with Rodbard using

386 the means of 3 independent examinations. The DC50 was estimated about 4 μM. **f,**

387 TUS-007 induced KRAS G12D chemical knockdown by 26S proteasome in a cell free

388 assay. KRAS G12D was incubated with 26S proteasome and agents as indicated for 3 h.

389 **Fig. 2. RAS chemical knockdown in cells.**

390 **a,** TUS-007 induced chemical knockdown was independent of ubiquitination. GFP

391 fused KRAS G12D and DsRed were transiently expressed in HeLa cells. The cells were

392 treated with TUS-007 in the presence of a proteasome inhibitor (MLN), a ubiquitination

393 inhibitor (NAEi) and a molecular chaperon inhibitor (HSP70 inhibitor: VER-155008)

394 for 24 h. **b & c,** RAS-less MEFs expressing KRAS G12D, G12V or G12C were

395 incubated with TUS-007 for 72 h. Representative blots of KRAS are shown (b). The

396 relative amounts of KRAS mutants normalized to GAPDH are shown in the bar graph

397 (mean ± SEM; n = 3–4). The cell viability was also measured (mean ± SEM; n = 3–4)

398 (g). *P < 0.05 and ** P < 0.01 vs. DMSO. TUS-007 induced chemical knockdown did

399 not cause non-specific cytotoxicity.

400

401 **Fig. 3. Chemical knockdown and tumor suppression *in vitro* and *in vivo* in KRAS**

402 **G12V-driven human colon cancer cells by TUS-007 treatment.**

403 **a,** Immunoblotting analysis of KRAS G12V chemical knockdown in SW620-Luc cells

404 treated with TUS-007 for 48 h at the indicated doses. The KRAS band intensity was

405 normalized to that of GAPDH (mean ± SEM; n = 3). *P < 0.05 and **P < 0.01 vs.

406 DMSO. **b & c,** The ratio of apoptotic cells were analyzed in colon cancer SW620-Luc

407 cells (**b**) and HT29-Luc cells (**c**), a KRAS-independent, BRAF-dependent cell line (Ctx

408 + Vem: 100 mg/ml cetuximab and 40 μM vemurafenib). Cells were treated with each

409 compound for 48 h in terms of the number of annexin V-positive/PI-negative apoptotic

410 cells detected by flow cytometry (mean ± SEM; n = 2–5). **P < 0.01, and ***P < 0.001

411 vs. DMSO. **d,** Relative activity of caspase 3/7 in SW620-Luc cells treated with TUS-

412 007 or 5-fluorouracil (5-FU) for 48 h (mean ± SEM; n = 3). *P < 0.05 and **P < 0.01

413 vs. DMSO. **e,** Tumor volume in mice with SW620-Luc cells transplanted

414 subcutaneously and treated with i.p. administration every 3 days (mean ± SEM; n = 6–

415 8). *P < 0.05 vs. vehicle alone. **f,** Tumors of SW620-Luc cells at day 21 from the same

416 mice shown in **e** (n = 6–8).

417

418 **Fig. 4. Chemical knockdown and tumor suppression *in vitro* and *in vivo* in KRAS**

419 **G12D-driven human pancreatic cancer cells by TUS-007 treatment.**

420 **a,** KRAS G12D chemical knockdown induced by TUS-007 in SW1990 cells. SW1990

421 cells were treated with TUS-007 for 72 h and analyzed by immunoblotting. The KRAS

422 G12D band intensity was normalized to that of GAPDH (mean ± SEM; n = 4). *P <

423 0.05 vs. DMSO. **b,** The proportion of annexin V-positive apoptotic SW1990 cells

424 treated with DMSO, RAS-SOS-NH_2 or TUS-007 for 72 h (mean ± SEM; n = 3). *P <

425 0.05 vs. DMSO or RAS-SOS-NH_2. **c,** TUS-007 increased the caspase 3/7 activity in

426 SW1990 cells after treatment for 96 h (mean ± SEM; n = 3). *P < 0.05 and **P < 0.01

427 vs. DMSO. **d,** Caspase 3/7 activation by TUS-007 was proteasome dependent and

428 ubiquitination independent. SW1990 cells were treated with the agents for 96 h (mean ±

429 SEM; n = 3). **P < 0.01 vs. DMSO, ##P < 0.01 vs. TUS-007 (100 μM) only, and †no

430 statistically significant difference compared with TUS-007 (100 μM) only. **e,** Tumor

431 volume in mice with SW1990 cells transplanted subcutaneously and treated with p.o.

432 administered TUS-007 or vehicle (mean ± SEM; n = 6–9). The agents were

433 administered every 3 days. **P < 0.01 vs. vehicle alone. **f,** Body weight changes in

434 mice with SW1990 cells transplanted subcutaneously (mean ± SEM; n = 6–9).

435

436 **Fig. 5. TUS-007 suppresses the growth of KRAS G12D-positive orthotopic**

437 **pancreatic tumors.**

438 **a,** Images showing the luciferase activity and total flux in orthotopic tumors

439 transplanted SW1990-Luc cells *in vivo*. **b,** Tumor growth (bioluminescence) in identical

440 mice treated with vehicle or TUS-007 administered p.o. every 3 days. (mean ± SEM; n

441 = 6). *P < 0.05 vs. vehicle alone. **c,** Representative histochemical staining of KRAS and

442 TUNEL in orthotopic tumor sections from the same mice used in **a**. The scale bar is 60

443 μm. **d,** Immunoblotting of KRAS G12D in tumor lysates from the same mice used in **a**.

444 The bar graph shows quantification of KRAS G12D normalized to GAPDH (mean ±

445 SEM; n = 6). **P < 0.01 vs. vehicle alone.

446

447 **Fig. S1. The heat resistance of KRAS G12D/V incubated with TUS-007.**

448 **a,** Evaluation of the target-binding affinity of TUS-007 to KRAS mutants by a thermal

449 shift assay. Recombinant KRAS was treated with the vehicle, RAS-SOS inhibitor, or

450 TUS-007 for 30 min, heated at the indicated temperature for 20 min, then analyzed by

451 immunoblotting. **b,** The means of T_m values from fluorescence-based thermal shift

452 assay shown in Fig. 1d. (mean ± SEM; n = 2). *P < 0.05 vs. DMSO, #P < 0.05 vs. RAS-

453 SOS inhibitor.

454

455 **Fig. S2. Effects of TUS-007 on proteasome activity levels.**

456 The levels of chymotrypsin-like (β5), trypsin-like (β2), and caspase-like (β1)

457 proteasome activities was monitored by Suc-LLVY-AMC, Bz-VGR-AMC, and Z-LLE-

458 AMC, respectively. AMC fluorescence was monitored by a plate reader with excitation

459 and emission filters of 360 and 460 nm, respectively (DMSO, 30 min = 1) (mean ±

460 SEM; n = 2–3).

461

462 **Fig. S3. TUS-007 induced degradation of KRAS G12V in cell free assay.**

463 Successful KRAS G12V degradation by TUS-007. KRAS G12V protein was incubated

464 with TUS-007 at the indicated concentrations in the presence of 26S proteasome for 1 h

465 (mean ± SEM; n = 3). *P < 0.05 vs. DMSO.

466

467 **Fig. S4. Selective chemical knockdown of RAS variants in RAS-less MEFs**

468 **expressing different types of human RAS.**

469 **a,** Relative viability of RAS-less MEFs expressing WT human RAS family members

470 after incubation with TUS-007 or DMSO. (mean ± SEM; n = 3–5). *P < 0.05 and **P <

471 0.01 vs. DMSO. **b,** Degradation of WT human RAS family members in RAS-less MEFs

472 treated with TUS-007 or DMSO for 72 h (mean ± SEM; n = 4–5). *P < 0.05 and **P <

473 0.01 vs. DMSO.

474

475 **Fig. S5. FACS plots for Annexin V- PI staining of SW620-Luc cells.**

476 SW620-Luc cells were treated with the indicated agents for 48 h, followed by staining

477 with Annexin V-FITC and PI. The typical plots are shown.

478

479 **Fig. S6. FACS plots for Annexin V- PI staining of HT29-Luc cells.**

480 HT29-Luc cells were treated with the indicated agents for 48 h, followed by staining

481 with Annexin V-FITC and PI. The typical plots are shown.

482

483 **Fig. S7. TUS-007 induced apoptosis only when KRAS degradation was detected in**

484 **KRAS G12V driven cancer cells.**

485 SW620-Luc cells were treated with TUS-007 for 12 h (mean ± SEM; n = 3). The left

486 axis indicates KRAS/GAPDH, and the right axis indicates relative ratio of apoptotic

487 cells. *P < 0.05 vs. DMSO. The ratio of KRAS/GAPDH was determined by image

488 analyses of immunoblotting and ration of apoptotic cells were measured using FACS.

489

490 **Fig. S8. Effects of TUS-007 on the growth of colon cancer subcutaneous xenografts**

491 **and toxicity.**

492 **a,** Comparison of SW620-Luc tumor weight at 21 days after injection (mean ± SEM; n

493 = 6–8). *P < 0.05 vs. vehicle alone. **b,** Immunoblotting of KRAS G12V chemical

494 knockdown in tumors from the same mice used in Fig. 2e (mean ± SEM; n = 6). **P <

495 0.01 vs. vehicle alone. **c,** Body weight changes in mice with SW620-Luc cells

496 transplanted subcutaneously (mean ± SEM; n = 6–8).

497

498 **Fig. S9. TUS-007 induced apoptosis only when KRAS degradation was detected in**

499 **KRAS G12D driven cancer cells.**

500 SW1990 cell were treated with TUS-007 for 12 h (mean ± SEM; n = 3). The left axis

501 indicates KRAS/GAPDH, and the right axis indicates relative ratio of apoptotic cells.

502 *P < 0.05 vs. DMSO. The ratio of KRAS/GAPDH was determined by image analyses

503 of immunoblotting and ration of apoptotic cells were measured using FACS.

504

505 **Fig. S10. Effects of TUS-007 on the growth of pancreatic cancer subcutaneous**

506 **xenografts and toxicity.**

507 **a,** Tumors of SW1990 cells from the same mice shown and comparison of tumor weight

508 in Fig. 3e at 21 days after p.o. administration (mean ± SEM; n = 6–9). *P < 0.05 vs.

509 vehicle alone. **b,** Tumor volume in mice with SW1990 cells transplanted

510 subcutaneously and treated with i.p. administered TUS-007 or vehicle (mean ± SEM; n

511 = 6–9). The agents were administered every three days. *P < 0.05 vs. vehicle. **c,** Body

512 weight changes in mice with SW1990 cells transplanted subcutaneously (mean ± SEM;

513 n = 6–9).

514

515 **Fig. S11. Effects of oral treatment with TUS-007 on wild type RAS in pancreas.**

516 The immunoblotting analyses of wt RAS proteins in pancreas from the same mice

517 shown in Fig. 3e (mean ± SEM; n = 6–9). *P < 0.05 vs. vehicle alone.

518

519 **Fig. S12. Effect of TUS-007 on RAS signaling in pancreatic cancer subcutaneous**

520 **xenografts.**

521 Immunoblotting of KRAS and downstream signaling molecules in tumors from the

522 same mice used in Fig. 3e (**a**: p.o. treatment) and Fig. S. 10c (**b**: i.p. treatment). The

523 quantitative analysis of the immunoblotting was shown as bar graph, where the KRAS

524 values were normalized to GAPDH, the p-ERK values were normalized to the total

525 ERK, and the p-AKT values were normalized to the total AKT (mean ± SEM; n = 6).

526 *P < 0.05 vs. vehicle.

527

528 **Fig. S13. Effect of TUS-007 on growth of orthotopic pancreatic cancer xenografts**

529 **expressing mutant KRAS.**

530 **a,** Tumor growth, as assessed by luciferase signal, in individual mice orthotopically

531 transplanted SW1990-Luc cells treated with TUS-007 (orange) or vehicle alone (blue)

532 (mean ± SEM; n = 6). **b,** Pancreases from orthotopic xenograft model mice at day 21

533 after treatment with TUS-007 (lower-left panel) or the vehicle alone (upper-left panel)

534 and comparison of their weights (right graph) (mean ± SEM; n = 6). *P < 0.05 vs.

535 vehicle alone. **c,** The quantitative analyses of the KRAS G12D-positive area (left) and

536 TUNEL-positive area (right) in Fig. 4c (mean ± SEM; n = 6). **P < 0.01 vs. vehicle

537 alone. **d,** Body weight changes in mice subjected to orthotopic transplantation of

538 SW1990-Luc cells (mean ± SEM; n = 6).

539

540 **Fig. S14. CANDDY induced degradation of MDM2, a common undruggable**

541 **target.**

542 **a,** The structure of MDM2-CANDDY using P53-MDM2 PPI inhibitor, with IC50 value

543 between 6-25 μM. **b,** MDM2-CANDDY degraded MDM2 in the dose dependent

544 manner. The human colon cancer cells HCT-116 were incubated for 48 h with MDM2-

545 CANDDY (mean ± SEM; n = 3). **P < 0.01 vs. DMSO.

546

547 **Table S1. The concentration of TUS-007 in pancreas was maintained for 72 h.**

548 The concentration of TUS-007 in pancreas from healthy wild-type mice i.p. treated with

549 TUS-007 at 80 mg/kg (means ± SEM; n = 5). The samples were obtained at indicated

550 time points after i.p. injection. The concentration of TUS-007 was measured with

551 HPLC.

552

553 **Table S2. Body weight change in toxicological tests.**

554 TUS-007 did not affected on the body weight changes of mice.

555

556 **Table S3. Weight of organs in toxicological tests.**

557 TUS-007 did not affected on the organ weight of mice.

558

559 **Table S4. Histological observations of organs in toxicological tests.**

560 TUS-007 did not cause histological changes in mice.

561

562 **Table S5. Hematology in toxicological tests.**

563 TUS-007 did not cause hematological changes in mice.

564

565 **Table S6. Biochemical examinations in toxicological tests.**

566 TUS-007 did not cause biochemical changes in mice.

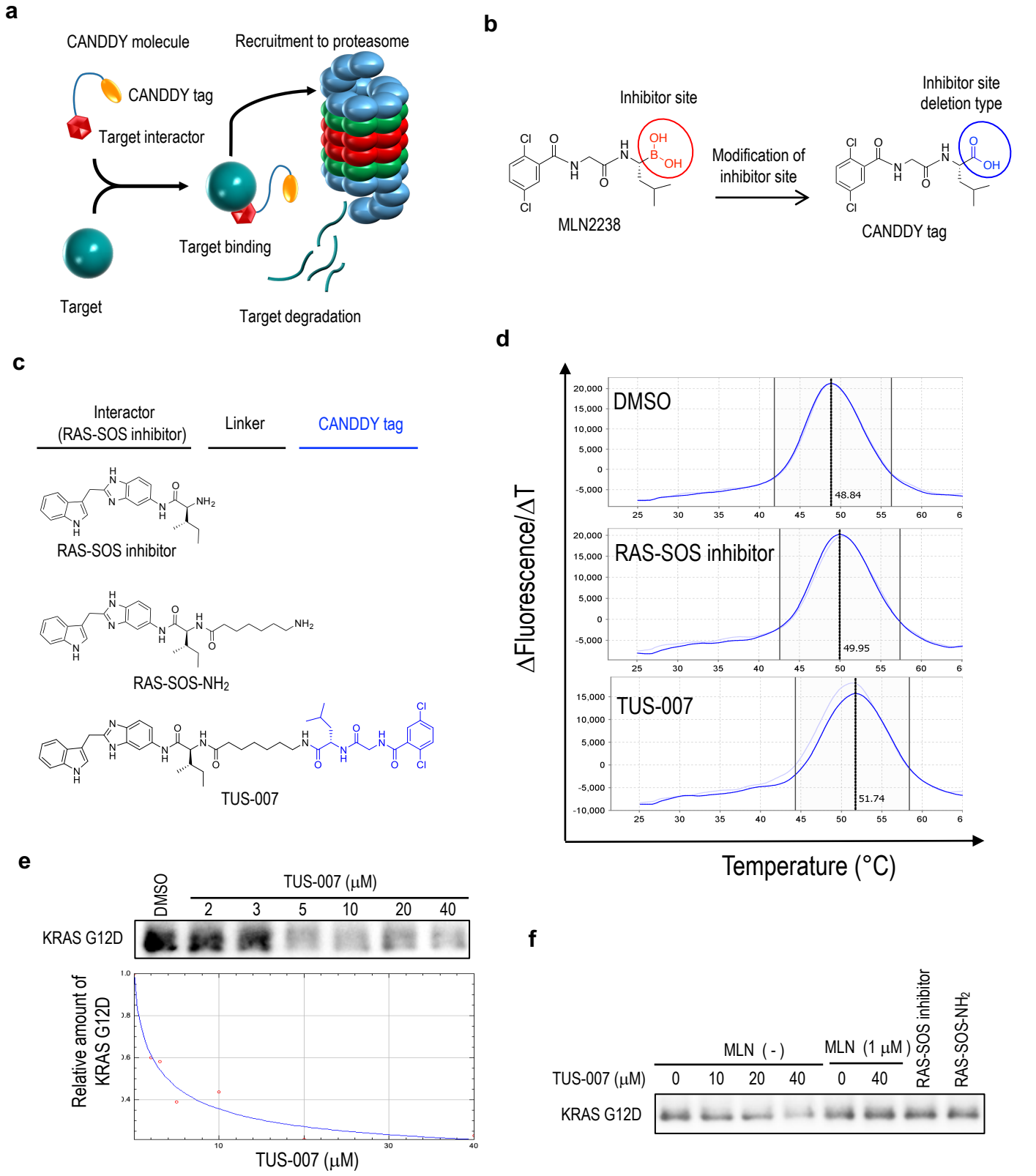

Fig. 1. RAS chemical knockdown in cell free assays.
a, Principle of the CANDDY technology. Each CANDDY molecule includes a target interactor (burgundy hexagon) and a CANDDY tag (yellow oval). The target protein is bound by the CANDDY molecule *via* the target interactor and is directly degraded by proteasome via the CANDDY tag. **b,** The CANDDY tag was synthesized by chemically inactivating the inhibitor site of MLM2238 (MLN). **c,** Structures of the RAS-SOS inhibitor (ref. 5), RAS-SOS-NH_2, and TUS-007. **d,** KRAS G12D was mixed with DMSO, RAS-SOS inhibitor (4 μM) or TUS-007 (4 μM) and incubated under heating from 25 °C to 99 °C. The denature of KRAS G12D was monitored by the fluorescence. The typical curve of each group was shown. **e,** The correlation between relative amount of KRAS G12D and concentration of TUS-007 were approximated with Rodbard using the means of 3 independent examinations. The DC50 was estimated about 4 μM. **f,** TUS-007 induced KRAS G12D chemical knockdown by 26S proteasome in a cell free assay. KRAS G12D was incubated with 26S proteasome and agents as indicated for 3 h.

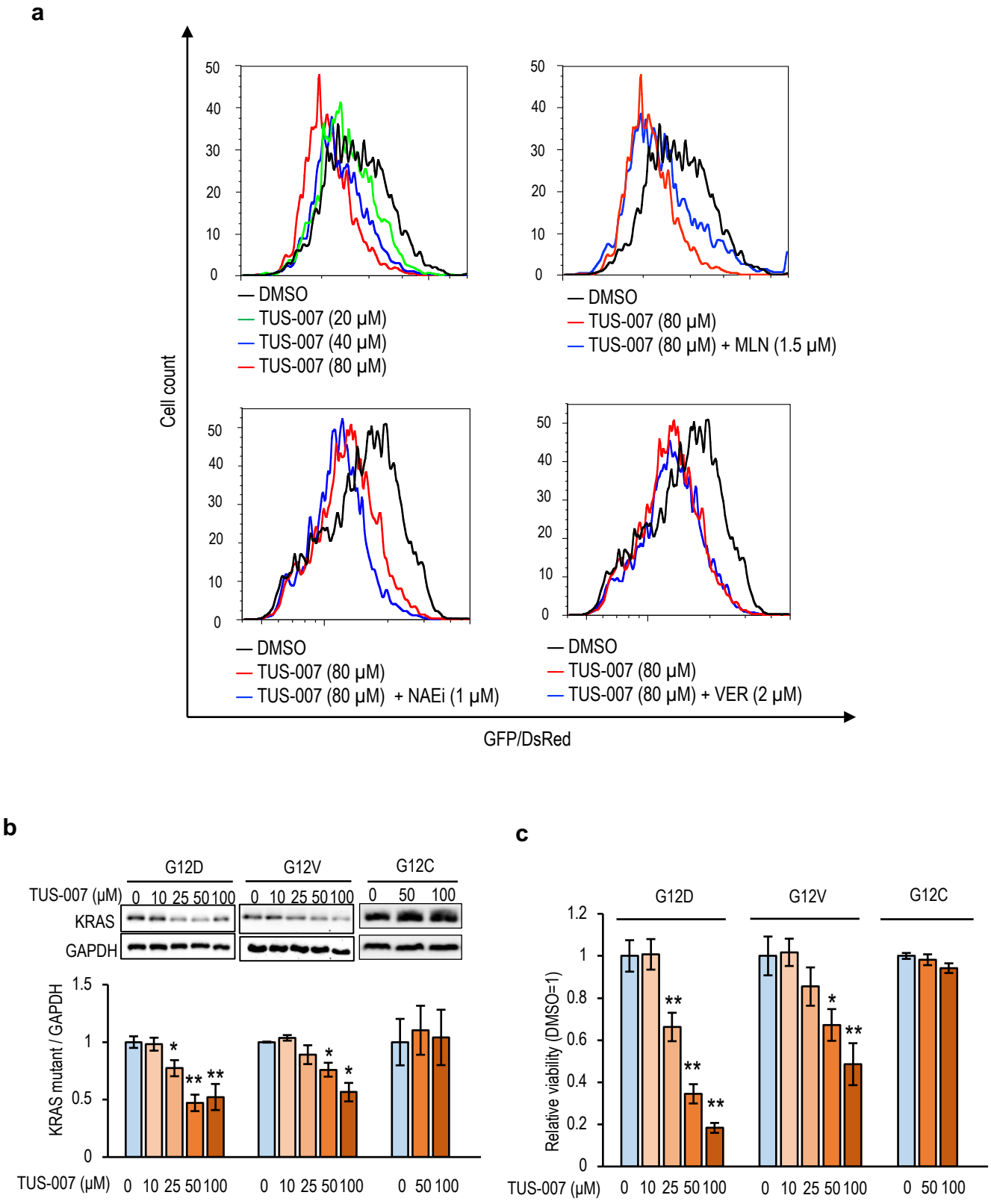

Fig. 2. RAS chemical knockdown in cells.

a, TUS-007 induced chemical knockdown was independent of ubiquitination**.** GFP fused KRAS G12D and DsRed were transiently expressed in HeLa cells. The cells were treated with TUS-007 in the presence of a proteasome inhibitor (MLN), a ubiquitination inhibitor (NAEi) and a molecular chaperon inhibitor (HSP70 inhibitor: VER-155008) for 24 h. **b & c,** RAS-less MEFs expressing KRAS G12D, G12V or G12C were incubated with TUS-007 for 72 h. Representative blots of KRAS are shown (**b**). The relative amounts of KRAS mutants normalized to GAPDH are shown in the bar graph (mean ± SEM; n = 3–4). The cell viability was also measured (mean ± SEM; n = 3–4) (**g**). *P < 0.05 and ** P < 0.01 vs. DMSO. TUS-007 induced chemical knockdown did not cause non-specific cytotoxicity.

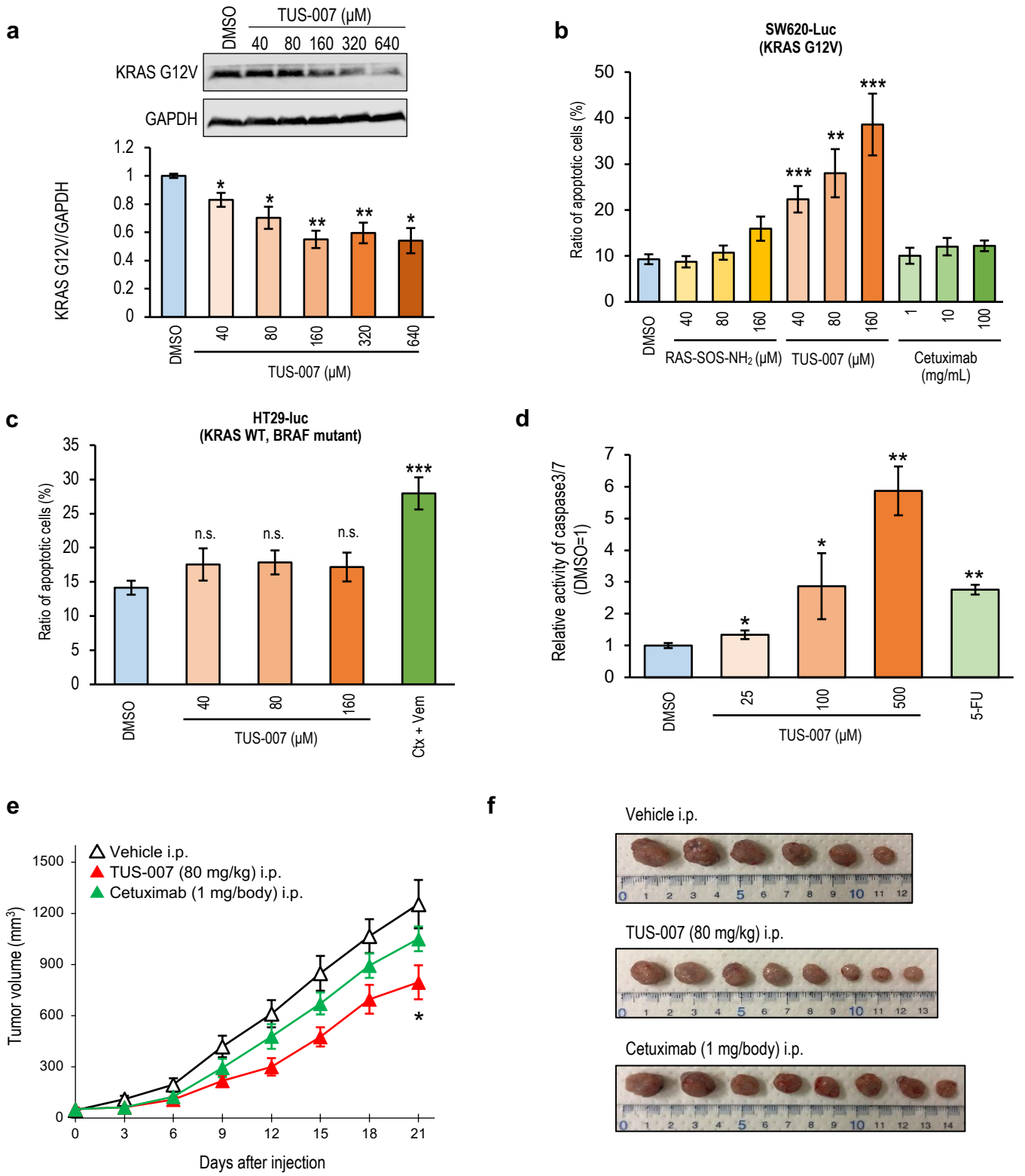

Fig. 3. Chemical knockdown and tumor suppression *in vitro* and *in vivo* in KRAS G12V-driven human colon cancer cells by TUS-007 treatment.

a, Immunoblotting analysis of KRAS G12V chemical knockdown in SW620-Luc cells treated with TUS-007 for 48 h at the indicated doses. The KRAS band intensity was normalized to that of GAPDH (mean ± SEM; n = 3). *P < 0.05 and **P < 0.01 vs. DMSO. **b & c,** The ratio of apoptotic cells were analyzed in colon cancer SW620-Luc cells (**b**) and HT29-Luc cells (**c**), a KRAS-independent, BRAF-dependent cell line (Ctx + Vem: 100 μg/ml cetuximab and 40 μM vemurafenib). Cells were treated with each compound for 48 h in terms of the number of annexin V-positive/PI-negative apoptotic cells detected by flow cytometry (mean ± SEM; n = 2–5). **P < 0.01, and ***P < 0.001 vs. DMSO. **d,** Relative activity of caspase 3/7 in SW620-Luc cells treated with TUS-007 or 5-fluorouracil (5-FU) for 48 h (mean ± SEM; n = 3). *P < 0.05 and **P < 0.01 vs. DMSO. **e,** Tumor volume in mice with SW620-Luc cells transplanted subcutaneously and treated with i.p. administration every 3 days (mean ± SEM; n = 6–8). *P < 0.05 vs. vehicle alone. **f,** Tumors of SW620-Luc cells at day 21 from the same mice shown in **e** (n = 6–8).

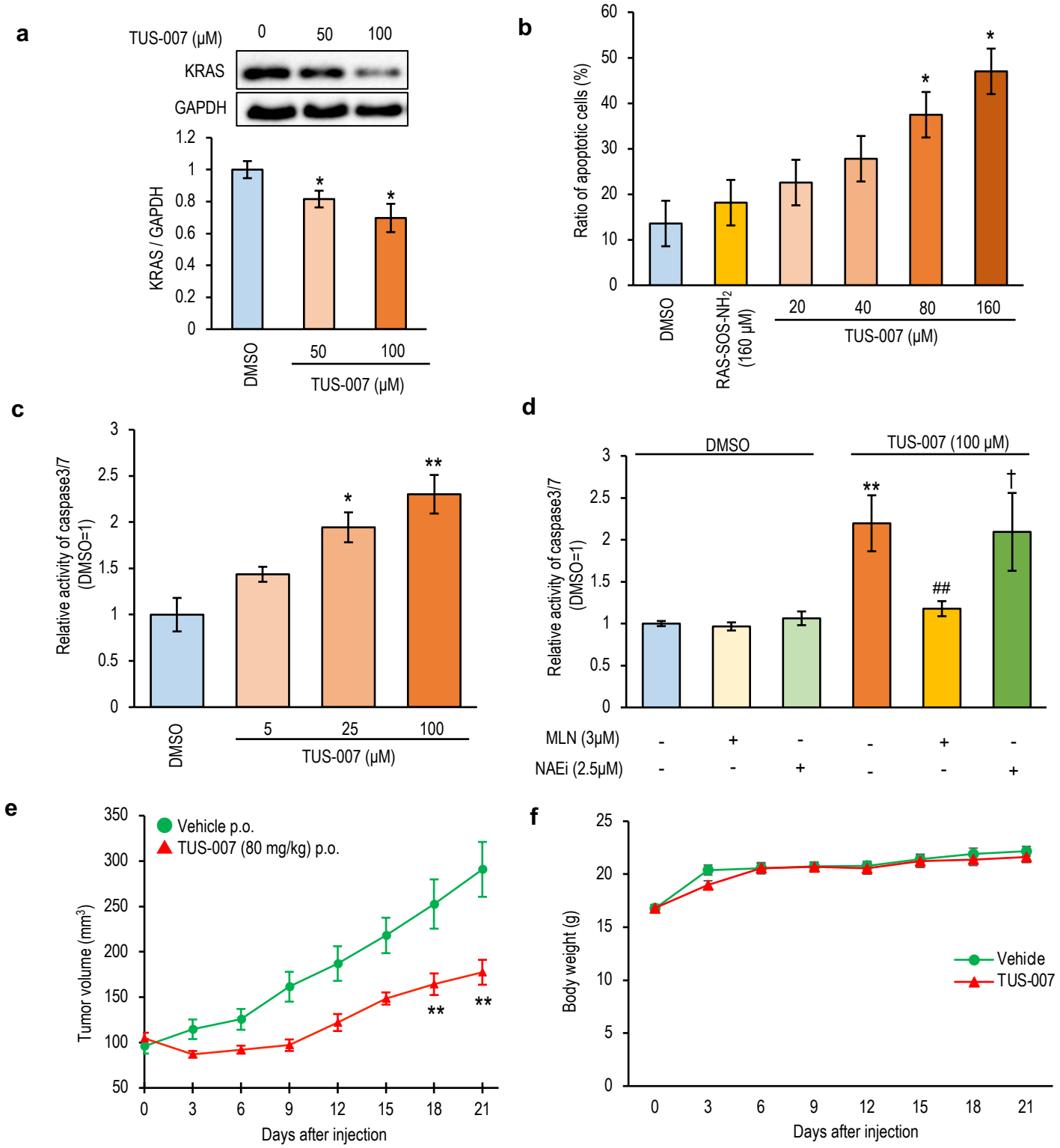

Fig. 4. Chemical-knockdown and tumor suppression *in vitro* and *in vivo* in KRAS G12D-driven human pancreatic cancer cells by TUS-007 treatment.

a, KRAS G12D chemical knockdown induced by TUS-007 in SW1990 cells. SW1990 cells were treated with TUS-007 for 72 h and analyzed by immunoblotting. The KRAS G12D band intensity was normalized to that of GAPDH (mean ± SEM; n = 4). *P < 0.05 vs. DMSO. **b,** The proportion of annexin V-positive apoptotic SW1990 cells treated with DMSO, RAS-SOS-NH_2 or TUS-007 for 72 h (mean ± SEM; n = 3). *P < 0.05 vs. DMSO or RAS-SOS-NH_2. **c,** TUS-007 increased the caspase 3/7 activity in SW1990 cells after treatment for 96 h (mean ± SEM; n = 3). *P < 0.05 and **P < 0.01 vs. DMSO. **d,** Caspase 3/7 activation by TUS-007 was proteasome dependent and ubiquitination independent. SW1990 cells were treated with the agents for 96 h (mean ± SEM; n = 3). **P < 0.01 vs. DMSO, ##P < 0.01 vs. TUS-007 (100 μM) only, and †no statistically significant difference compared with TUS-007 (100 μM) only. **e,** Tumor volume in mice with SW1990 cells transplanted subcutaneously and treated with p.o. administered TUS-007 or vehicle (mean ± SEM; n = 6–9). The agents were administered every 3 days. **P < 0.01 vs. vehicle alone. **f,** Body weight changes in mice with SW1990 cells transplanted subcutaneously (mean ± SEM; n = 6–9).

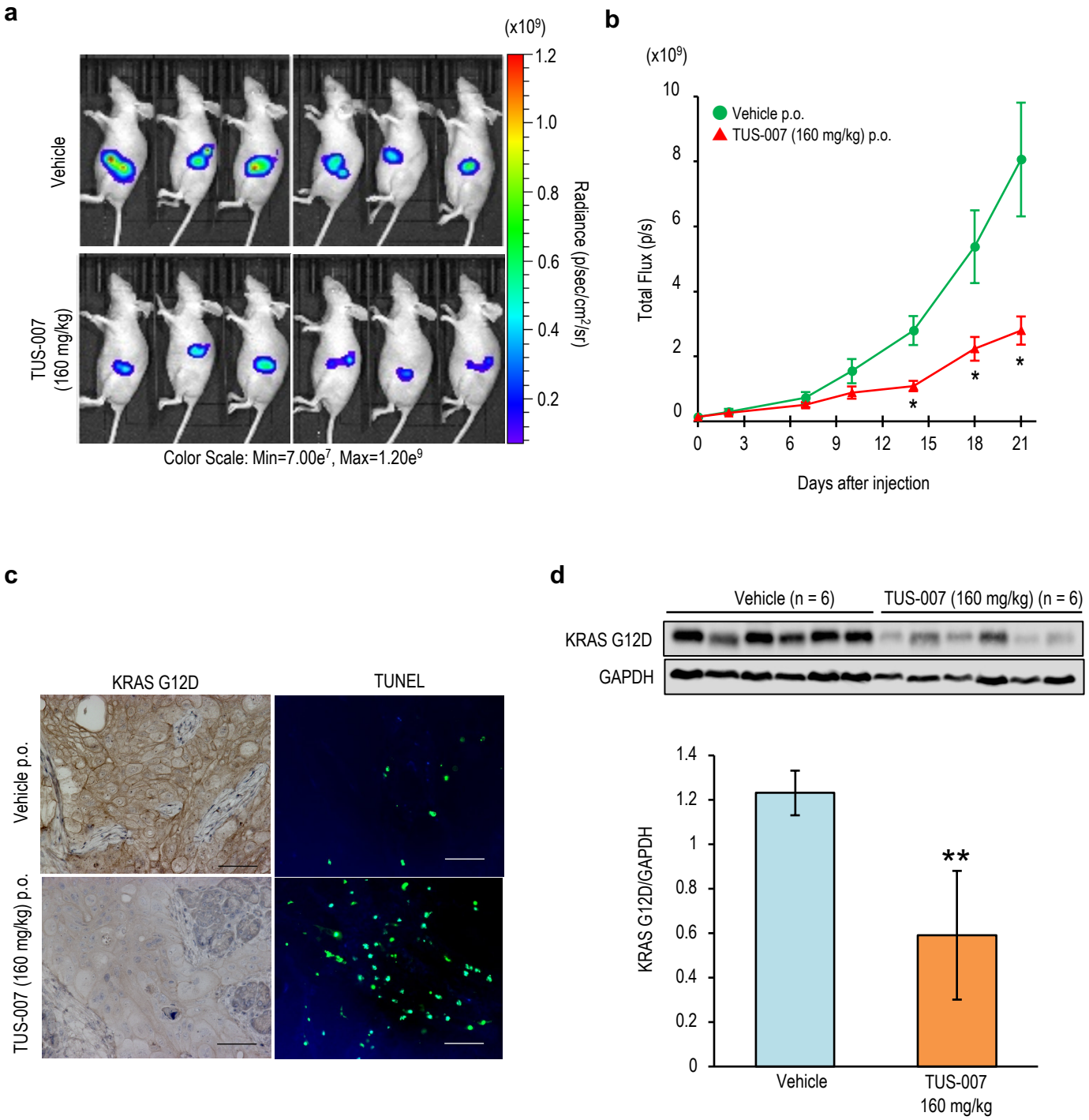

Fig. 5. TUS-007 suppresses the growth of KRAS G12D-positive orthotopic pancreatic tumors.
a, Images showing the luciferase activity and total flux in orthotopic tumors transplanted SW1990-Luc cells *in vivo*. **b,** Tumor growth (bioluminescence) in identical mice treated with vehicle or TUS-007 administered p.o. every 3 days. (mean ± SEM; n = 6). *P < 0.05 vs. vehicle alone. **c,** Representative histochemical staining of KRAS and TUNEL in orthotopic tumor sections from the same mice used in **a**. The scale bar is 60 μm. **d,** Immunoblotting of KRAS G12D in tumor lysates from the same mice used in **a**. The bar graph shows quantification of KRAS G12D normalized to GAPDH (mean ± SEM; n = 6). **P < 0.01 vs. vehicle alone.

1 **Supplementary Information for "*In vivo* KRAS G12D/V degradation mediated by**

2 **CANDDY using a modified proteasome inhibitor"**

3 Satoshi Imanishi, Lijuan Huang, Shoko Itakura, Masamichi Ishizaka, Yoichi Iwasaki,

4 Tomohiro Yamaguchi, and Etsuko Miyamoto-Sato.

5

Materials and methods

Cell lines. SW1990 and HCT-116 cells were purchased from the American Type Culture Collection (Manassas, VA, USA). SW620-Luc and HT29-Luc cells were purchased from the National Institute of Biomedical Innovation, Health, and Nutrition (Osaka, Japan). RAS-less MEF cell lines (wild-type (wt) KRAS, KRAS G12D, KRAS G12V, KRAS G12C, NRAS and HRAS) were obtained from the National Institutes of Health (NCI RAS Initiative at the Frederick National Laboratory for Cancer Research, Frederick, MD, USA).

Animal studies. BALB/cA-nu/nu and BALB/cA (female, 7-9 weeks old) were purchased from CLEA Japan (Tokyo, Japan). The animals were maintained in conventional housing conditions, with a daily 12-h light/dark cycle, and given food and water *ad libitum*. The animals were cared for in accordance with the NIH Guide for the Care and Use of Laboratory Animals. All animal experiments were approved by the Committee on Animal Experimentation of the Tokyo University of Science.

22

23 **Reagents.** MLN2238 (A10600) was purchased from AdooQ BioScience (Irvine, CA,

24 USA). NAEi was purchased from AdipoGen (San Diego, CA, USA). Human 26S

25 Proteasome Protein (E-365) and Human 20S Proteasome Protein (E-360) were

26 purchased from R&D Systems (Minneapolis, MN, USA). Human KRAS (G12D) and

27 the corresponding His tag (12259-H07E1) were purchased from Sino Biological

28 (Beijing, China). Human KRAS (G12V), 2-186, and the corresponding His tag

29 (R06-32BH) were obtained from SignalChem Lifesciences (Richmond, British

30 Columbia, Canada).

31

32 **Measurement of 20S proteasome activity.** The chymotrypsin-like (β5), trypsin-like

33 (β2), and caspase-like (β1) activities of the 20S proteasome were measured using a 20S

34 Proteasome Activity Kit GOLD (StressMarq Bioscience Inc., Victoria, British Columbia,

35 Canada). Purified 20S proteasome (0.1 μg) was incubated in the presence of CANDDY

36 molecules (1, 4, 10, 20, 40, 80, and 160 μM) or MLN2238 at the indicated

37 concentrations for 30 min at room temperature. After incubation, 100 mM of

38 fluorogenic peptide substrates, Suc-LLVY-AMC (β5 substrate), Bz-VGR-AMC (β2
39 substrate), or Z-LLE-AMC (β1 substrate), was added, followed by incubation for 1 h at
40 room temperature. The reaction mixture was then transferred to a 96-well plate, and the
41 fluorecence from hydrolyzed AMC groups was measured using a Synergy HT
42 multi-channel microplate reader (BioTek Instruments, Inc., Winooski, VT, USA) with a
43 360 nm excitation filter and 460 nm emission filter.
44
45 **Evaluation of affinity of TUS-007 for KRAS in a thermal shift assay.** The KRAS
46 G12D/V (100 nM) was preincubated with TUS-007, a RAS-SOS inhibitor, or 10%
47 DMSO in 75 mM phosphate buffer (pH 7.5) for 30 min at 37 °C (G12D) or for 20 min
48 at 25 °C (G12V). Aliquots of the reaction solution were sampled into separate
49 microtubes and heated for 30 min at 70, 80, or 90 °C for G12D, or at 40, 50, or 60 °C
50 for G12V. After centrifugation at 18,000 ×*g* for 20 min, the supernatants were analyzed
51 by SDS-PAGE, followed by immunoblotting using an anti-KRAS antibody (1:1000,
52 WH0003845MI, Sigma-Aldrich, St. Louis, MO, USA). Immunoreactive bands were
53 detected using an iBright CL1000 chemiluminator (Thermo Fisher Scientific, Waltham,

54 MA, USA) with an enhanced chemiluminescent substrate for detection of horseradish

55 peroxidase (HRP; Merck, Darmstadt, Germany).

56

57 **Estimation of T_m values using fluorescence based thermal shift assay.** To estimate

58 the T_m values, we performed a fluorescence based thermal shift assay using ProteoStat

59 Thermal Shift Stability assay (ENZO Life Sciences, Farmingdale, NY, USA). 1 μg of

60 KRAS G12D was mixed with DMSO (2.5 %), RAS-SOS inhibitor (4 μM) or TUS-007

61 (4 μM) in 1x assay buffer containing a fluorescent indicator of protein destabilization,

62 ProteoStat TS Detection Reagent, and incubated under heating from 25 °C to 99 °C in

63 StepOne Plus Real-time PCR system (Thermo Fisher Scientific). The kinetics of

64 fluorescent signals were analyzed to calculate T_m values in Protein Thermal Shift

65 Software 1.3 (Thermo Fisher Scientific).

66

67 **Evaluation of KRAS degradation induced by TUS-007 in a cell-free system.** KRAS

68 G12D (final concentration: 5 ng/μL) and 26S proteasome (final concentration: 8 nM)

69 were incubated with TUS-007 (2, 3, 5, 10, 20, 40 μM), RAS-SOS inhibitor (40 μM),

70 RAS-SOS-NH_2 (40 μM) or DMSO in 20 mM Tris-HCl buffer (pH 7.5) containing 20%

71 glycerol for 3 h at 37 °C. To assess the effect of MLN on chemical knockdown, KRAS

72 G12D and 26S proteasome were incubated with DMSO or TUS-007 40 μM in the

73 presence or absence of MLN (1 μM) in the same condition. KRAS G12V (final

74 concentration: 5 ng/μL) and 26S proteasome (final concentration: 8 nM) were incubated

75 with TUS-007 at the indicated concentration or DMSO in 75 mM phosphate buffer,

76 containing 1% LABRASOL (Gattefossé, Saint-Priest, France), for 1 h at 37 °C. After

77 centrifugation at 14,000 ×*g* for 10 min, the supernatants were analyzed by SDS-PAGE,

78 followed by immunoblotting using an anti-KRAS antibody (1:1000, WH0003845MI for

79 G12D, Sigma-Aldrich; and 1:2000, F234 for G12V, Santa Cruz Biotechnology, Inc.,

80 Dallas, TX, USA). The immunoreactive bands were detected, as described above. The

81 DC_{50} values were calculated by a Rodbard approximation using the band intensity

82 obtained from four and three independent experiments for G12D. Immunoblotting was

83 performed as mentioned above.

84

85 **Evaluation of target degradation in HeLa cells by flow cytometry.** The expression

86 plasmid pMIR-DsRed-IRES-ecDHFR-HA-GFP was a kind gift from Dr. L. Hedstrom
87 (Brandeis University). Plasmid expressing human KRAS G12D was constructed by RF
88 cloning with some minor modifications. A full-length cDNA clone of human KRAS
89 (AK292510) was obtained from the National Institute of Technology and Evaluation
90 (Tokyo, Japan). Hybrid RF cloning primers were designed using RF-Cloning.org. All
91 PCR amplifications were performed with KOD-Plus-Neo (Toyobo Co. Ltd., Japan). The
92 plasmid DNA sequences encoding target proteins were determined using an ABI 3500
93 (Applied Biosystems, MA, USA). HA-GFP-fusion target protein- and
94 DsRed-expressing HeLa cells were treated with 1% DMSO or CANDDY molecules in
95 serum-free medium for 24 h. The cells were harvested using trypsin and resuspended in
96 fluorescence activated cell sorter (FACS) buffer. The cells were then analysed on a BD
97 FACSCanto II. Data were analysed using FlowJo software (FlowJo LLC).
98
99 **Cell proliferation assay.** To examine the effect of TUS-007 on cell proliferation, the
100 WST-8 assay (Cell Count Reagent SF; Nacalai Tesque, Kyoto, Japan) was performed.
101 RAS-less MEF cells, expressing human RAS, were plated in 96-well plates at a density

102 of 3×10^3 cells per well, cultured overnight, then treated with the indicated
103 concentrations of TUS-007 in 4% FBS containing medium (KRAS G12D), 10% FBS
104 containing medium (KRAS G12V) or serum-free medium (KRAS G12C, wt KRAS,
105 HRAS, NRAS) for 72 h. After incubation, cell viability was measured
106 spectrophotometrically using the WST-8 reagent. The culture medium was removed and
107 WST-8 reagent was mixed with the growth medium at a ratio of 1:10 (with a final
108 volume of 110 μL) and added to each well. The cells were incubated in an atmosphere
109 of 5% CO_2 at 37 °C for 1 to 2 h, and the absorbance at 450 nm was measured using the
110 aforementioned Synergy HT multi-channel microplate reader (BioTek Instruments,
111 Inc.).
112
113 **Evaluation of TUS-007 specificity in cells.** RAS-less MEFs were used to evaluate the
114 selective degradation by TUS-007. RAS-less MEFs expressing one of the human WT
115 RAS members (KRAS WT, HRAS WT, or NRAS WT) or KRAS G12C were plated into
116 6-well plates at a density of 3×10^4 cells per well, cultured overnight, and treated with
117 the indicated concentrations of TUS-007 in serum-free medium for 72 h. RAS-less

118 MEFs expressing KRAS G12D or G12V were plated into 96-well plates at a density of
119 3×10^3 cells per well, cultured overnight, and treated with the indicated concentrations
120 of TUS-007 in 4% FBS or 10% FBS containing medium, respectively, for 72 h. The
121 cells were lysed using RIPA buffer (Nacalai Tesque., Kyoto, Japan). The lysates were
122 centrifuged at 18,000 ×*g* for 10 min. The supernatants were analyzed by western
123 blotting using mouse monoclonal antibodies specific to KRAS (1:1000,
124 WH0003845MI; Sigma-Aldrich) and glyceraldehyde 3-phosphate dehydrogenase
125 (GAPDH, 1:10000, sc-32233; Santa Cruz Biotechnology, Inc.) and rabbit polyclonal
126 antibodies specific for HRAS (1:1000, 18295-1-AP; Proteintech, Rosemont, IL, USA)
127 and NRAS (1:1000, 10724-1-AP, Proteintech). Immunoreactive bands were detected
128 using iBright CL1000 chemiluminator or LAS 3000 (Fujifilm, Tokyo, Japan) with an
129 enhanced chemiluminescent substrate for the detection of horseradish peroxidase (HRP;
130 Merck, Darmstadt, Germany). The intensity of the RAS band was quantified using
131 ImageJ software and normalized to the intensity of the GAPDH band.
132
133 **Measurement of KRAS protein levels in cells by western blotting.** SW620-Luc and

134 SW1990 cells were treated with 1% DMSO or TUS-007 in serum-free medium for 12

135 or 48 h (SW620-Luc cells) and 12 or 72 h (SW1990 cells). The cells were lysed using a

136 RIPA buffer (Nacalai Tesque., Kyoto, Japan). The precipitates were separated from the

137 soluble fraction by centrifugation at 18,000 ×*g* for 20 min. The supernatants were

138 analyzed by western blotting with mouse monoclonal antibodies specific for KRAS

139 (1:1000, WH0003845MI; Sigma-Aldrich) and GAPDH (1:20000, sc-32233; Santa Cruz

140 Biotechnology, Inc.). The immunoreactive bands were detected by LAS-3000, as

141 described above. The intensity of the KRAS band was quantified using ImageJ software

142 and normalized to the intensity of the GAPDH band.

143

144 **Evaluation of caspase activity.** To measure caspase activity, SW1990 cells were plated

145 onto 96-well white plates and 96-well clear plates, at a concentration of 8×10^3

146 cells/well, in a medium containing 10% FBS. The plates were incubated overnight

147 without CO_2 equilibration at 37 °C. The medium was replaced with medium containing

148 2% FBS, DMSO, 100 μM TUS-007, 3 μM MLN2238, or 2.5 μM NAEi and incubated

149 for 96 h. SW620-Luc cells were plated onto 96-well white plates and 96-well clear

150 plates at 2×10^3 cells/well in medium containing 10% FBS. After overnight incubation,

151 the medium was replaced with FBS-free medium containing 1% L-glutamine, DMSO,

152 and 25, 100, or 500 μM TUS-007 for 48 h. The caspase 3/7 Glo assay (Promega,

153 Madison, WI, USA) was performed on the white plates according to the manufacturer's

154 protocol. The chemiluminescence intensity was measured with a Synergy HT plate

155 reader (BioTek). The cell viability was measured in the clear plates using the WST-8

156 assay, as described above. Caspase 3/7 activity was obtained as the chemical

157 luminescence intensity of the caspase 3/7 Glo assay normalized to the cell viability.

158

159 **Analysis of apoptosis by flow cytometry.** SW1990, SW620-Luc, and HT-29 cells were

160 seeded in 24-well plates, followed by the addition of compounds at the indicated

161 concentrations. After incubation for 12 or 48 h (SW620-Luc, HT-29) and 12 or 72 h

162 (SW1990), the cells were harvested using trypsin, washed with phosphate-buffered

163 saline (PBS), and pelleted by centrifugation at 110 $\times g$ for 5 min. The cells were

164 resuspended in 85 μL of binding buffer (Annexin V-FITC Kit, Medical & Biological

165 Laboratories Co., Ltd., Nagoya, Japan). Subsequently, 10 μL of annexin V-FITC and 5

166 μL of propidium iodide (PI) were added to each sample, followed by incubation in the

167 dark at room temperature for 15 min. After incubation, 400 μL of binding buffer was

168 added to each sample on ice. The cells were then analyzed using a FACSCanto II

169 fluorescence-activated cell sorter (BD Biosciences, Santa Clara, CA, USA) to detect the

170 fluorescein isothiocyanate (FITC) signal with excitation and emission filter wavelengths

171 of 488 nm and 580 nm, respectively, to detect the PI signal. Data were analyzed using

172 FlowJo software (FlowJo, Eugene, OR, USA).

173

174 **Subcutaneous xenograft model.** SW620-Luc (3×10^7 cells/mL) and SW1990 (5×10^7

175 cells/mL) cells were suspended in PBS, and 100 μL of the single-cell suspension was

176 transplanted subcutaneously into the right flanks of BALB/cA-nu/nu mice using a 26 G

177 syringe. Tumor volumes were calculated as the tumor length × width^2 × 0.5. When the

178 tumor volumes reached approximately 100 mm^3, the mice were randomized into

179 treatment and control groups of 6 to 8 animals per group. For i.p. treatment, TUS-007

180 was dissolved in DMSO and then diluted to a final concentration of 10% DMSO in 20%

181 polyethylene glycol (PEG) 400/Tween 80 (1:1 ratio). The TUS-007 solution was

182 administered intraperitoneally into the tumor-bearing mice at a dose of 80 mg/kg every
183 three days. The control mice were treated with the PEG/Tween vehicle alone. For p.o.
184 treatment, TUS-007 was suspended in 0.5% (w/v) carboxymethyl cellulose (CMC) and
185 administered p.o. at a dose of 80 mg/kg every three days. CMC (0.5% w/v) was
186 administered to control mice. Cetuximab was administered to an additional group of
187 SW620-Luc-implanted mice at a dose of 1 mg/mouse every three days.
188
189 **Orthotopic xenograft model.** The pGL4.51 (Luc2/CMV/Neo) vector (Promega) was
190 transfected into SW1990 cells. Successfully transfected cells were selected using G418.
191 SW1990-Luc cells were mixed with growth factor-reduced Matrigel (BD Biosciences)
192 on ice, at a ratio of 1:1 (v/v), to obtain a final cell density of 1.5×10^4 cells/μL. Ten
193 microliters of the cell suspension was injected directly into the pancreas of
194 BALB/cA-nu/nu mice using a 27 G syringe. Three days after cell transplantation,
195 TUS-007 treatment was initiated in six mice. TUS-007 was suspended in 0.5% (w/v)
196 CMC and administered orally at a dose of 160 mg/kg every 3 days. CMC (0.5% w/v)
197 was administered to control mice (n = 6). Tumor luciferase activity was monitored

198 based on the bioluminescence intensity. Fifty microliters of D-luciferin (30 mg/mL in
199 saline) was injected subcutaneously in mice (Promega). Twenty minutes after the
200 injection, bioluminescence images were obtained using an IVIS Lumina LT (Perkin
201 Elmer, Waltham, MA, USA) with an exposure time of 15 s while the mice were under
202 isoflurane anesthesia (Wako, Tokyo, Japan).
203
204 **Measurement of RAS levels and downstream signaling molecule activation in**
205 **xenograft tumors.** KRAS expression in xenograft tumors and wt RAS protein
206 expression in pancreas were evaluated by immunohistochemistry and western blot
207 analysis. Tumor tissue and pancreas were harvested from the mice harboring
208 subcutaneous xenografts on day 21 of the TUS-007 administration. Tumor tissues were
209 harvested from the orthotopic xenograft mice on day 24 after the TUS-007
210 administration for consecutive 3 days starting on day 21. A portion of each sample was
211 fixed in 4% paraformaldehyde (Nacalai Tesque., Kyoto, Japan), embedded in paraffin,
212 then cut into 5 μm-thick sections. The sections were deparaffinized and incubated in
213 0.3% hydrogen peroxide in methanol for 30 min, and antigen retrieval was performed

214 using a 10 mM citrate buffer (pH 6.0) at 121 °C for 20 min. Tumor tissues were
215 subsequently blocked with 1% bovine serum albumin (BSA) in PBS for 30 min and
216 stained with primary antibodies specific for human KRAS (1:200, 12063-1-AP;
217 Proteintech), diluted in 1% BSA, followed by HRP-labeled secondary antibodies (1:600,
218 ab6721; Abcam, Cambridge, UK) in 1% BSA for 30 min at room temperature. The
219 sections were counterstained with hematoxylin and visualized with diaminobenzidine
220 (1.02924.0001; Merck). Digital images were obtained at 40× magnification using a
221 model BZ-9000 microscope (Keyence, Osaka, Japan). The area of KRAS staining was
222 quantified using ImageJ software, and the perimeter-to-area ratio (KRAS-positive
223 area/section) was calculated for a total of 30 images of 6 tumor sections from each
224 group. The remaining part of each tumor sample was homogenized in a cell-lysis buffer
225 (50 mM triethanolamine, 50 mM KCl, 5 mM $MgCl_2$, 0.25 M sucrose, 1 mM
226 phenylmethylsulfonyl fluoride, proteinase inhibitors (Nacalai Tesque., Kyoto, Japan), 1
227 mM dithiothreitol, and ribonuclease inhibitor (0.2 unit/μl, TaKaRa Bio., Shiga, Japan)
228 for western blot analysis, as described above. Mouse monoclonal antibodies specific for
229 KRAS (1:1000, WH0003845MI; Sigma-Aldrich), HRAS (1:1000, 18295-1-AP;

230 Proteintech, Rosemont, IL, USA), NRAS (1:1000, 10724-1-AP, Proteintech) and
231 GAPDH (1:20000, sc-32233; Santa Cruz Biotechnology, Inc.) and rabbit antibodies
232 specific for p-Erk1/2 (phospho-p44/42 MAPK) (1:1000, #4370; Cell Signaling
233 Technology, Beverly, MA, USA), Erk1/2 (p44/42 MAPK) (1:1000, #4695; Cell
234 Signaling Technology), p-Akt (1:2000, #4060; Cell Signaling Technology), and Akt
235 (1:2000; #4691; Cell Signaling Technology) were used for the immunohistochemical
236 staining. The immunoreactive bands were detected by LAS-3000 as described above.
237 Quantitative analysis of the western blots was performed using ImageJ software, and the
238 results were normalized to the GAPDH band intensity.
239
240 **Measurement of apoptosis in xenograft tumors.** DNA fragmentation in the tumor
241 tissues was evaluated by a TdT-mediated dUTP nick-end labeling (TUNEL) assay.
242 Paraffin-embedded tissue sections (5 μm thick) were deparaffinized. The TUNEL
243 reaction was performed using the DeadEnd Fluorometric TUNEL System (Promega),
244 according to the manufacturer's instructions. Fluorescence images were acquired using a
245 BZ-9000 fluorescence microscope (Keyence). TUNEL-positive cells were identified

246 and counted using ImageJ software. In total, 30 images of 6 tumor sections were

247 analyzed from each group.

248

249 **Determination of TUS-007 in pancreas.** BALB/cA mice were treated i.p. with

250 TUS-007, and pancreas tissue was collected at suitable time points. Approximately

251 30-60 mg of tissue was homogenized in 0.6 mL of tissue-lysis buffer (50 mM Tris-HCl

252 pH 8.0, 20 mM EDTA, 10 mM NaCl, 1% SDS) by Micro Smash MS-100 using

253 stainless (5.5 ϕ) and zirconia (1.0 ϕ) beads (TOMY SEIKO CO., LTD., Tokyo, Japan),

254 and 1 μL propyl p-hydroxybenzoate (4 mg/mL in DMSO) was added to each sample as

255 an internal standard. Lysates were centrifuged at 18,000 ×*g* for 10 min and 2.25 mL of

256 methanol/chloroform (ratio of 2:1) was added to the supernatants and the mixture was

257 allowed to stand for 30 min at room temperature. Chloroform and distilled water (0.75

258 mL each) were added and samples were centrifuged at 1,500 ×*g* for 15 min. The layer of

259 chloroform was collected. The supernatants were dried under reduced pressure and

260 redissolved in the mobile phase. TUS-007 was determined by HPLC (Alliance e2695,

261 Waters Corporation., MA, USA) using COSMOSIL® C18-AR-II column (150×4.6 mm,

262 Nacalai Tesque., Kyoto, Japan) in the isocratic elution mode with 0.1% trifluoroacetic
263 acid (TFA) in 50:50 (v/v) acetonitrile/water mobile phase at a flow rate of 1.0 mL/min.
264 All reagents for the assay were purchased from Nacalai Tesque. (Kyoto, Japan).
265
266 **Toxicity tests of TUS-007 in mice.** The male ICR mice (6 weeks old) were
267 administrated vehicle solution (0.5% CMC containing 2.5% DMSO) or TUS-007
268 dissolved vehicle at 80 mg/kg for continuous 5 days. The observation of general
269 conditions was performed every day up to Day 17. The body weight was measured at
270 Day 0, 1, 2, 3, 4, 6, 8, 10, 12, 15 and 17. At Day 17, the organs and blood were collected
271 under isoflurane anesthesia. The organs were immediately fixed in 10% phosphate
272 buffered formalin and embedded in paraffin for histological examination after HE
273 staining. The blood cells were analyzed by FACS (ADVIA2120i, Siemens Healthineers
274 AG, Germany.) and the blood biochemical examinations were performed using
275 automatic analyzer TBA-120FR (CANON MEDICAL SYSTEMS Co., Ltd., Tochigi,
276 Japan). Statistical analyses were performed with SAS Release 9.1.3 (SAS Institute Inc.,
277 NC, USA).

278

279 **Degradation of MDM2 in HCT-116 cells.** HCT-116 human colon-cancer cells were

280 treated with 1% DMSO or TUS-007 in serum-free medium for 24 h. The cells were

281 lysed using a RIPA buffer (Nacalai Tesque). The precipitates were separated from the

282 soluble fraction by centrifugation at 18,000 ×*g* for 20 min. The supernatants were

283 analyzed by western blotting using a rabbit polyclonal antibody specific for MDM2

284 (1:1000, sc-965, Santa Cruz Biotechnology, Inc.) and GAPDH (1:20000, sc-32233;

285 Santa Cruz Biotechnology, Inc.). The immunoreactive bands were detected by

286 LAS-3000, as described above. The intensity of the MDM2 band was quantified using

287 ImageJ software and normalized to the intensity of the GAPDH band.

288

289 **Statistical analyses.** Statistical significance was determined with JMP® Pro 14 (SAS

290 Institute Inc., Cary, NC, USA). An unpaired *t*-test was used to compare pairs of groups

291 under the assumption of normality. A one-way ANOVA with Dunnett's post hoc analysis

292 was used to compare sets of three or more groups. P-values < 0.05 were considered

293 statistically significant.

294

295 **Text S1. Synthesis of CANDDY molecules.**

296 **General**. Nuclear magnetic resonance (NMR) spectra were recorded on a Bruker

297 BioSpin AVANCE600 spectrometer operating at 600 MHz for ^{1}H-NMR. Chemical shifts

298 were reported in the scale relative to CD_3OD as an internal reference. Fast-atom

299 bombardment mass spectrometry was performed on a JEOL JMS-700. Column

300 chromatography was performed with silica gel 60 (75 mm) purchased from Nacalai

301 Tesque, Inc. PLC silica gel 60 was purchased from Merck KGaA. Reversed phase liquid

302 chromatography was performed with high performance liquid chromatography (HPLC)

303 (Shimadzu Co., Ltd), with a YMC-Pack ODS-A or Inertsil ODS-4 (GL Science) (250 ×

304 4.6 mm), an LC-6AD pump, and a RID-10A detector (Shimadzu Co., Ltd). HPLC

305 experiment was performed with isocratic condition A (MeCN/H_2O/TFA, 70:30:0.1; flow

306 rate, 1 mL/min) for compounds **1–3**, and condition B (MeCN/H_2O/TFA, 55:45:0.1; flow

307 rate, 1 mL/min) for TUS-007.

308 H-Gly-OtBu · HCl and 2,5-dichlorobenzoic acid were purchased from Ark Pharm.

309 H-Leu-OtBu · HCl and H-Phe-OtBu · HCl were purchased from Watanabe Chemical

310 Industry.

311 Synthesis of TMP-NH_2 was based on a previous report[26]. The synthesis of RAS-SOS

312 inhibitor (**4**) and RAS-SOS-NH_2 (**5**) was based on a previous report[15]. A part of the

313 compound was synthesized by NARD Institute. Ltd. (Kobe, Japan).

314

315 **The synthesis of TUS-007.**

316 TUS-007 was synthesized as shown below.

317 Some of the compounds were synthesized by the NARD Institute. Ltd. (Kobe, Japan).

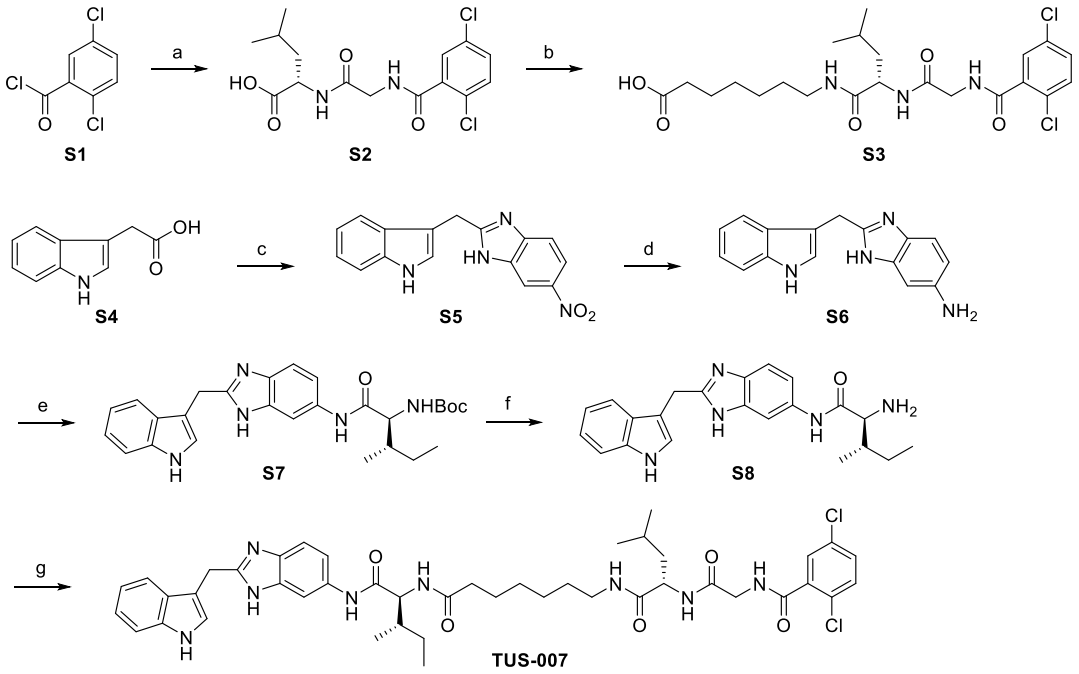

Reagent and conditions: (a) Glycyl-L-luecine, 1N NaOHaq.,THF 0°C, 88%; (b) (i) HOSu, EDC-HCl, CH_2Cl_2, 0°C to rt, (ii) 7-Amino-heptanoic acid, Triethylamine, DMF, 0°C to rt, 72%; (c) (i) CDI, THF, 0°C to rt; 4-Nitro-1,2-phenylenediamine, 47°C, (ii) AcOH, reflux, 88%; (d) H_2, Pd/C, MeOH, rt, 62%; (e) *N*-Boc-L-Isoleucine, COMU, DIPEA, MeCN, 0°C to rt, *quant.*; (f) TFA, CH_2Cl_2, rt, 76%; (g) **S3**, HATU, DIPEA, DMF, 0°C to rt, 53%.

318

319 To a solution of glycyl-L-leucine (125 g, 664 mmol) in 1N NaOH*aq*. (1.3 L)

320 with tetrahydrofuran (THF: 550 mL), 2,5-dichlorobenzoyl chloride (127 g, 604 mmol)

321 in THF (250 mL) was added dropwise at 0°C. After stirring for 2 h at the same

322 temperature, the resulting solution was acidified (ca. pH2) with 2N HCl*aq*. and

323 extracted with $CHCl_3$ (total 3 L). The combined organic layer was washed with brine,

324 dried over $MgSO_4$, filtered, and concentrated *in vacuo*. The residue was suspended in

325 diisopropyl ether (IPE: 1.2 L) and stirred for 30 min at 50°C. The resulting suspension

326 was cooled to room temperature, and a precipitate was filtered, washed with IPE (500

327 mL), and thus **S2** (194 g, 88 % yield, white solid) was obtained.

328 (i) To a solution of **S2** (194g, 536 mmol) in CH_2Cl_2 (1.6 L), *N*-hydroxysuccinimide

329 (HOSu: 2.5 g, 804 mmol) and 1-ethyl-3-(3-dimethylaminopropyl) carbodiimide

330 hydrochloride (EDC-HCl: 54 g, 804 mmol) were added at 0°C under Ar atmosphere.

331 After stirring for 3 h at room temperature, the resulting solution was washed with water

332 (1 L) three times, dried over $MgSO_4$, filtered, and concentrated *in vacuo*. (ii) The

333 residue (309 g) was dissolved in DMF (1.5 L) at Ar atmosphere, and 7-aminoheptanoic

334 acid (77.8 g, 536 mmol) and triethylamine (178 mL) were added to the solution at 0°C.

335 After stirring overnight at room temperature, 1N HCl*aq*. (1.5 L), water (1 L) and AcOEt

336 (3 L) were added and extraction was performed using AcOEt (1.5 L). The combined

337 organic layer was dried over Na_2SO_4, filtered, concentrated *in vacuo* and azeotroped

338 with toluene. The residue (394 g) was purified by silica gel column chromatography

339 (4.5 kg, elution with 0-5 % MeOH/$CHCl_3$) and thus **S3** (190 g, 72 % yield, white solid)

340 was obtained. **S3**: ^{1}H-NMR (400 MHz, DMSO-d_6) δ 0.84 (3H, d, J = 6.4 Hz), 0.87 (3H,

341 d, J = 6.4 Hz), 1.18-1.27 (4H, m), 1.35-1.60 (7H, m), 2.16 (2H, t, J = 7.3 Hz), 2.94-3.09

342 (2H, m), 3.82-3.92 (2H, m), 4.26-4.31 (1H, m), 7.53 (3H, s), 7.92 (1H, t, J = 5.5 Hz),

343 7.96 (1H, d, J = 8.2 Hz), 8.78 (1H, t, J = 6.0 Hz), 11.96 (1H, s).

344 (i) To a solution of indol-3-ylacetic acid (100 g, 571 mmol) in THF (200 mL),

345 1,1'-Carbonyldiimidazole (CDI: 109 g, 674 mmol) was added in portions over 15 min at

346 0°C under Ar atmosphere. After stirring for 30 min at room temperature,

347 4-nitro-1,2-phenylenediamine (96.2 g, 628 mmol) was added, and stirred for 30 min at

348 same temperature. The resulting solution was warmed to 47°C and concentrated *in*

349 *vacuo* after stirring overnight. (ii) The residue was dissolved in AcOH (2 L) with

350 ice-cooling and heated to reflux for 2 h. The resulting solution was concentrated *in*

351 *vacuo* and azeotroped with toluene. The residue was dissolved in AcOEt (1 L), and

352 insoluble portion was filtered on a Celite-pad, then washed with AcOEt (0.8 L). The

353 filtrate was washed with water (1.5 L) and brine (1 L), dried over Na_2SO_4, and

354 concentrated *in vacuo*. The residue (298 g) was purified by silica gel column

355 chromatography (2 kg, elution with 0-30 % AcOEt/$CHCl_3$) and thus **S5** (146 g, 88 %

356 yield, brown amorphous) was obtained.

357 To a solution of **S5** (146 g, 500 mmol) in MeOH (1 L), Pd/C (20.0 g) was added and

358 stirred overnight at room temperature under H_2 atmosphere. The resulting solution was

359 filtered on a Celite-pad, washed with MeOH (2 L), and concentrated *in vacuo*. The

360 residue was purified by silica gel column chromatography (3.0 kg, elution with 5-20 %

361 MeOH/$CHCl_3$) and thus **S6** (85.4 g, 62 % yield, black solid) was obtained.

362 To a solution of **S6** (81.9 g, 351 mmol) in MeCN (1.2 L), *N*-ethyldiisopropylamine

363 (DIPEA: 119 mL) and (1-Cyano-2-ethoxy-2-oxoethylidenaminooxy)dimethylamino-

364 morpholinocarbenium Hexafluorophosphate (COMU: 58 g, 368 mmol) were added at

365 0°C under Ar atmosphere, and stirred for 1 h at room temperature. After cooling to 0°C,

366 *N*-Boc-isoleucine (89.4 g, 341 mmol) was added and stirred overnight at room

367 temperature, and then concentrated *in vacuo*. The residue was diluted with $CHCl_3$ (2 L)

368 and washed with water (1.5 L) twice, concentrated *in vacuo*, and thus **S7** (330 g, *quant*.,

black oil) was obtained. This compound was used in the next step without further purification.

To a solution of **S7** (330 g) in CH_2Cl_2 (1.6 L), trifluoroacetic acid (TFA: 800 mL) was added at room temperature under Ar atmosphere and stirred for 2 h at the same temperature. The resulting solution was concentrated *in vacuo*, and then dissolved in AcOEt (1 L), washed with *sat*. $NaHCO_3$*aq*. (600 mL) twice, dried over Na_2SO_4, filtered, and concentrated *in vacuo*. The residue (315 g) was purified by NH-silica gel column chromatography (2.3 kg, elution with 0-5 % MeOH/$CHCl_3$), and thus **S8** (97.5 g, 76 % yield, yellow solid) was obtained.

To a solution of **S3** (139 g, 285 mmol) in *N*,*N*-dimethylformamide (DMF: 1250 mL), DIPEA (77.1 mL) and 1-[bis(dimethylamino)methylene]-1*H*-1,2,3-triazolo[4,5-*b*]pyridinium 3-oxide hexafluorophosphate (HATU: 109 g, 259 mmol) were added at 0°C under Ar atmosphere. After stirring for 30 min at the same temperature, **S8** (97.4 g, 259 mmol) was added at 0°C and stirred overnight at room temperature. The resulting solution was diluted with AcOEt (2.5 L) and water (1.5 L) and extracted with AcOEt (1.5 L). The

385 combined organic layer was concentrated *in vacuo* and azeotroped with toluene. The

386 residue (448 g) was purified by NH-silica gel (6.0 kg, elution with 0-4 %

387 MeOH/$CHCl_3$) and concentrated *in vacuo*. After dissolving in MeOH (500 mL),

388 insoluble was filtered off and the filtrate was concentrated *in vacuo*. The residue was

389 suspended in Me_2CO (1.5 L), stirred, and cooled to room temperature. Subsequently, a

390 precipitate was collected, and thus **TUS-007** (117 g, 53 % yield, yellow solid) was

391 obtained.**TUS-007**: ^{1}H-NMR (400 MHz, DMSO-d_6) δ 0.83 (3H, d, J = 6.4 Hz),

392 0.74-0.88 (6H, m), 0.87 (3H, d, J = 6.4 Hz), 1.08-1.28 (5H, m), 1.36-1.59 (8H, m),

393 1.75-1.82 (1H, m), 2.07-2.21 (2H, m), 2.94-3.08 (2H, m), 3.81-3.92 (2H, m), 4.22-4.38

394 (4H, m), 6.89-6.93 (1H, m), 7.02-7.06 (1H, m), 7.14-7.44 (4H, m), 7.34 (1H, d, J = 8.2

395 Hz), 7.52 (3H, s), 7.88-7.97 (4H, m), 8.78 (1H, t, J = 5.7 Hz), 9.96 (1H, d, J = 22.4 Hz),

396 10.92 (1H, s), 11.93-11.97 (1H, m). HR-MS (FAB) *m/z*: 845.3674 (Calcd for

397 $C_{44}H_{55}Cl_2N_8O_5$ $[M+H]^+$ 845.3672).

398

399 **The synthesis of MDM2-CANDDY.**

400 MDM2-CANDDY was synthesized as shown below. Some of the compounds were

401 synthesized by the NARD Institute. Ltd. (Kobe, Japan).

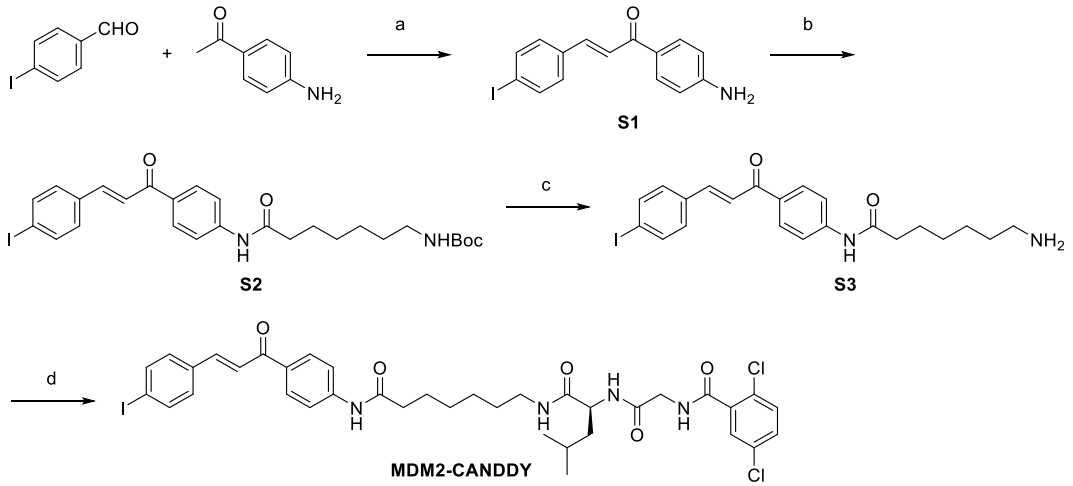

402 Reagent and conditions: (a) 40% KOHaq., EtOH, 0°C to rt, 60%; (b) 7-{(*tert*-Butoxycarbonyl)amino}heptanoic acid, HATU, DIPEA, DMAP, DMA/CH_2Cl_2, 0°C to rt, 70%; (c) TFA, CH_2Cl_2, 0°C, 99%; (d) CANDDY-MLN, HATU, DIPEA, DMF/CH_2Cl_2, 0°C to rt, 65%.

403 To a solution of 4-Iodobenzaldehyde (7.00 g, 30.1 mmol) and 4′-Aminoacetophenone

404 (4.08 g, 30.1 mmol) in EtOH (90 mL), 40% KOH*aq*. (60 mL) was added dropwise over

405 1 h at 0°C and stirred for 1 h under Ar atmosphere. After stirring for 6 h at room

406 temperature, the resulting solution was cooled to 12°C. A precipitate was collected by

407 filtration and washed with EtOH-water (1:2, 80 mL). The collected solid was dissolved

408 in $CHCl_3$ (800 mL) and the insoluble content was filtered and removed. The filtrate was

409 washed with water twice, dried over Na_2SO_4, filtered, concentrated *in vacuo*, and thus

410 **S1** (6.27 g, 60% yield, yellow solid) was obtained. This compound was used without

411 further purification.

412 To a solution of **S1** (6.16 g, 17.7 mmol), 7-{(*tert*-Butoxycarbonyl)amino}heptanoic acid

413 (4.35 g, 17.7 mmol), and DIPEA (4.62 mL, 26.5 mmol) in CH_2Cl_2-*N*,*N*-dimethyl-

414 acetamide (DMA: 10:1, 170 mL), HATU (10.2 g, 26.8 mmol) was added at 0°C under

415 Ar atmosphere. After stirring for 1 h at the same temperature, the solution was warmed

416 to room temperature and stirred for 4 h, and then 4-dimethylaminopyridine (DMAP:

417 250 mg, 2.04 mmol) was added, and stirred further 17 h at ambient temperature. After

418 stirring for 48 h at 30°C, the resulting solution was diluted with CH_2Cl_2 (1.2 L) and

419 washed with water (0.6 L), 1N HClaq. (0.6 L) twice, sat. $NaHCO_3$aq. (0.6 L) and brine

420 (0.6 L). The combined organic layer was dried over Na_2SO_4, filtered, and concentrated

421 in vacuo. The residue was purified by silica gel column chromatography (elution with

422 10-50% AcOEt/heptane). Next, the resulting rough solid was suspended in AcOEt (150

423 mL) at 50°C for 1 h and IPE (300 mL) was added, and the mixture was cooled on

424 ice-bath. A precipitate was collected, and thus **S2** (7.14 g, 70% yield, pale yellow solid)

425 was obtained.

426 To a solution of **S2** (2.50 g, 4.34 mmol) in CH_2Cl_2 (125 mL), TFA (63 mL) was

427 added at 0°C under Ar atmosphere. After stirring 1.5 h at the same temperature, the

428 resulting solution was concentrated *in vacuo*. The residue was dissolved in CH_2Cl_2,

429 poured into sat. $NaHCO_3$aq./water (2:1, 300 mL) and stirred for 1 h. The precipitate was

430 collected by filtration, washed with water (20 mL) twice, dried *in vacuo*, and thus **S3**

431 (2.05g, 99% yield, pale orange solid) was obtained.

432 To a solution of **CANDDY_MLN** (MLN2238 derived CANDDY tag: 0.72 g, 2.0 mmol,

433 synthesized by WO2018092723) in DMF/CH_2Cl_2 (1:1, 20 mL), DIPEA (0.32 mL, 1.9

434 mmol) and HATU (0.76 g, 2.0 mmol) were added at 3°C. After stirring at same

435 temperature for 30 min, **S3** (0.90g, 1.9 mmol) was added and warmed to room

436 temperature, stirred for further 3 h at room temperature. The resulting solution was

437 evaporated, diluted with water (200 mL), and stirred. A precipitate was collected by

438 filtration, dried *in vacuo*, and thus **MDM2-CANDDY** (1.0 g, 65% yield, white solid)

439 was obtained. **MDM2-CANDDY**: ^{1}H-NMR (400 MHz, DMSO-d_6) δ 0.84 (3H, d, *J* =

440 6.5 Hz), 0.87 (3H, d, *J* = 6.5 Hz), 1.25-1.31 (4H, m), 1.38-1.46 (4H, m), 1.53-1.59 (3H,

441 m), 2.33 (2H, t, *J* = 7.2 Hz), 2.97-3.07 (2H, m), 3.81-3.91 (2H, m), 4.25-4.31 (1H, m),

442 7.52 (3H, s), 7.64 (1H, d, *J* = 15.8 Hz), 7.67 (2H, d, *J* = 8.5 Hz), 7.76 (2H, d, *J* = 8.9

443 Hz), 7.82 (2H, d, *J* = 8.5 Hz), 7.91-7.98 (2H, m), 7.96 (1H, d, *J* = 15.8 Hz), 8.12 (2H, d,

444 *J* = 8.9 Hz), 8.78 (1H, dd, *J* = 5.9, 5.9 Hz), 10.23 (1H, s). HR-MS (FAB) *m/z*: 819.1577

445 (Calcd for $C_{37}H_{42}Cl_2IN_4O_5$ $[M+H]^+$ 819.1577).

Supplementary Figures for **"*In vivo* KRAS G12D/V degradation mediated by CANDDY using a modified proteasome inhibitor"**.

Satoshi Imanishi, Lijuan Huang, Shoko Itakura, Masamichi Ishizaka, Yoichi Iwasaki, Tomohiro Yamaguchi, and Etsuko Miyamoto-Sato

a

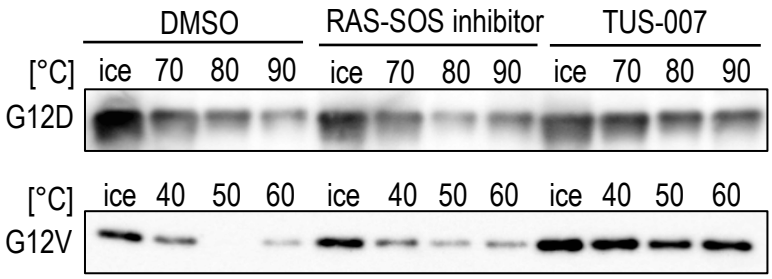

b

	T_m (°C)
DMSO	48.8 ± 0.05
RAS-SOS inhibitor	50.1 ± 0.15*
TUS-007	51.5 ± 0.2*,#

Fig. S1. The heat resistance of KRAS G12D/V incubated with TUS-007.
a, Evaluation of the target-binding affinity of TUS-007 to KRAS mutants by a thermal shift assay. Recombinant KRAS was treated with the vehicle, RAS-SOS inhibitor, or TUS-007 for 30 min, heated at the indicated temperature for 20 min, then analyzed by immunoblotting. **b,** The means of T_m values from fluorescence-based thermal shift assay shown in Fig. 1d. (mean ± SEM; n = 2). *P < 0.05 vs. DMSO, #P < 0.05 vs. RAS-SOS inhibitor.

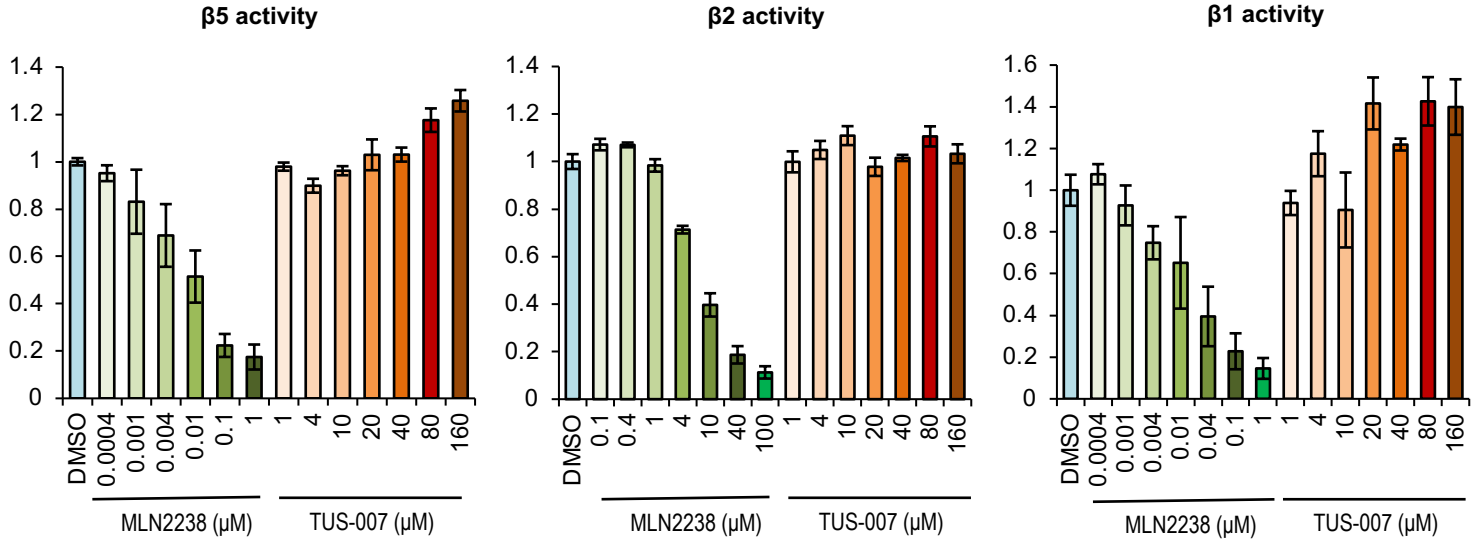

Fig. S2. Effects of TUS-007 on proteasome activity levels.
The levels of chymotrypsin-like (β5), trypsin-like (β2), and caspase-like (β1) proteasome activities was monitored by Suc-LLVY-AMC, Bz-VGR-AMC, and Z-LLE-AMC, respectively. AMC fluorescence was monitored by a plate reader with excitation and emission filters of 360 and 460 nm, respectively (DMSO, 30 min = 1) (mean ± SEM; n = 2–3).

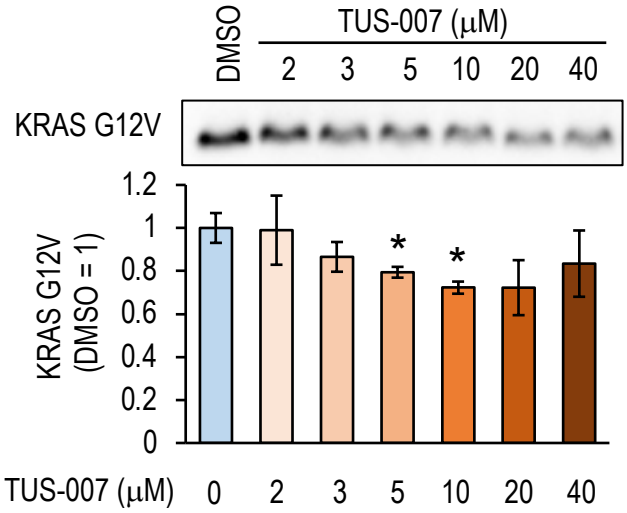

Fig. S3. TUS-007 induced degradation of KRAS G12V in cell free assay.
Successful KRAS G12V degradation by TUS-007. KRAS G12V protein was incubated with TUS-007 at the indicated concentrations in the presence of 26S proteasome for 1 h (mean ± SEM; n = 3). *P < 0.05 vs. DMSO.

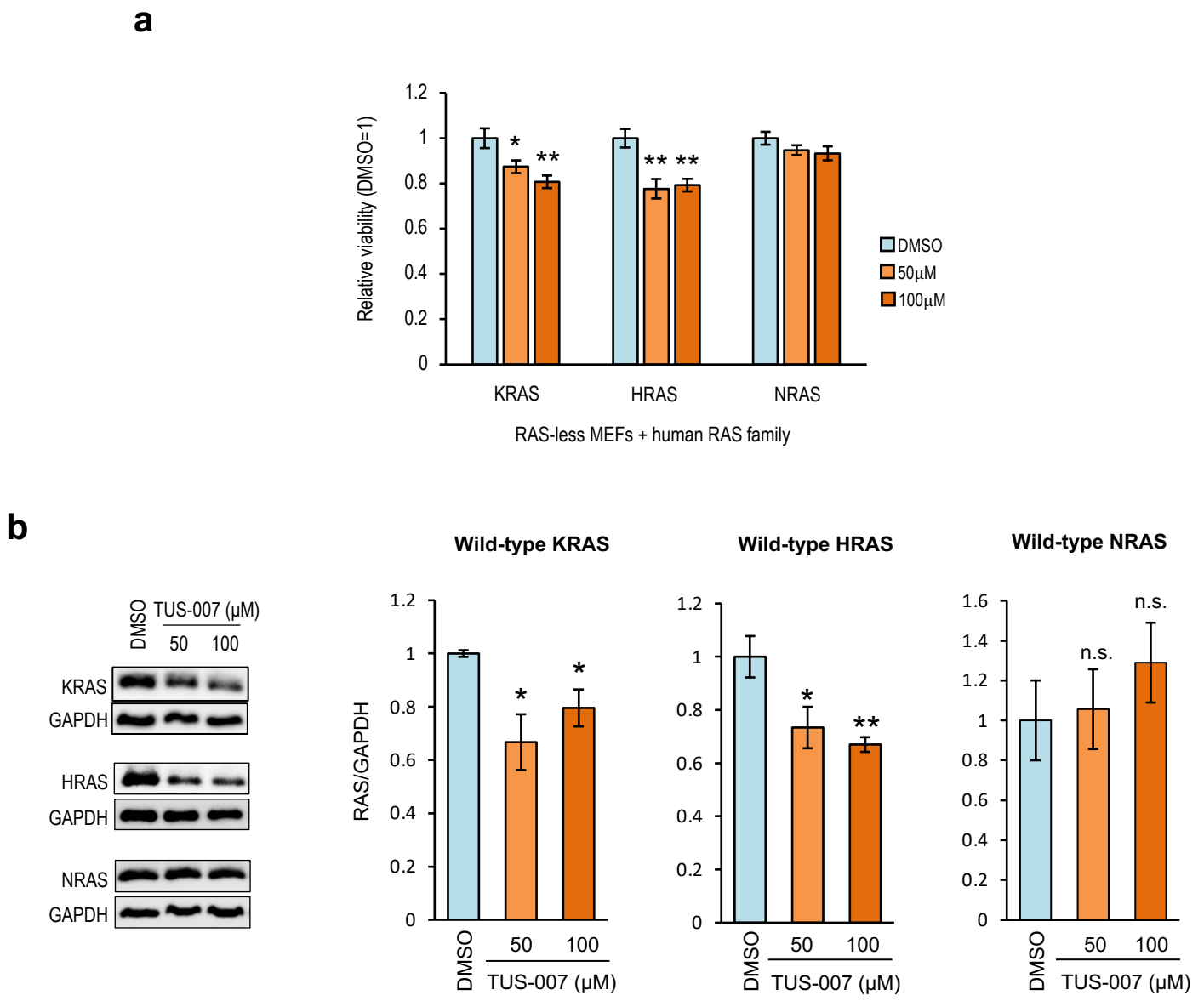

Fig. S4. Selective chemical-knockdown of RAS variants in RAS-less MEFs expressing different types of human RAS. a, Relative viability of RAS-less MEFs expressing WT human RAS family members after incubation with TUS-007 or DMSO. (mean ± SEM; n = 3–5). *P < 0.05 and **P < 0.01 vs. DMSO. **b,** Degradation of WT human RAS family members in RAS-less MEFs treated with TUS-007 or DMSO for 72 h (mean ± SEM; n = 4–5). *P < 0.05 and **P < 0.01 vs. DMSO.

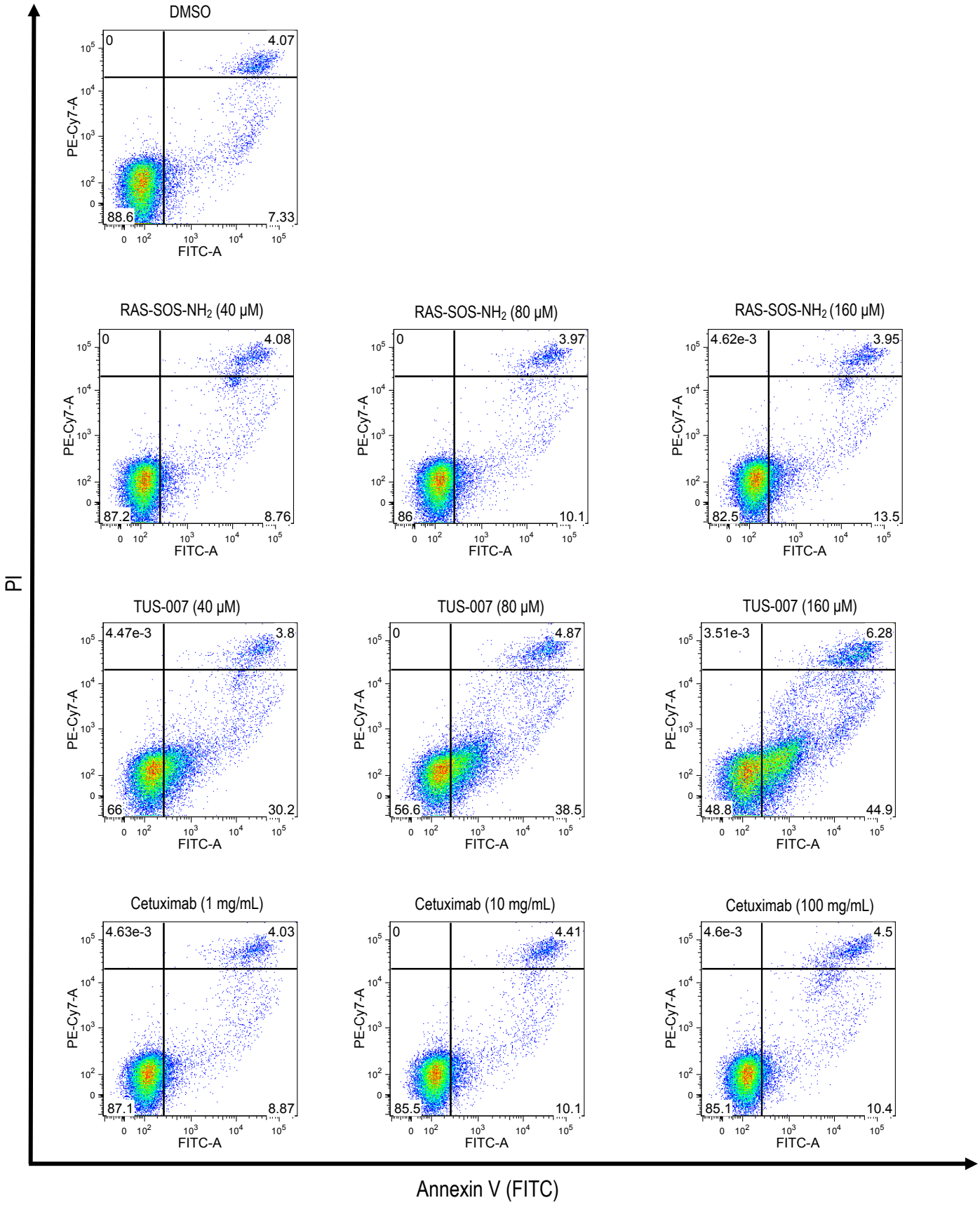

Fig. S5. FACS plots for Annexin V- PI staining of SW620-Luc cells.
SW620-Luc cells were treated with the indicated agents for 48 h, followed by staining with Annexin V-FITC and PI. The typical plots are shown.

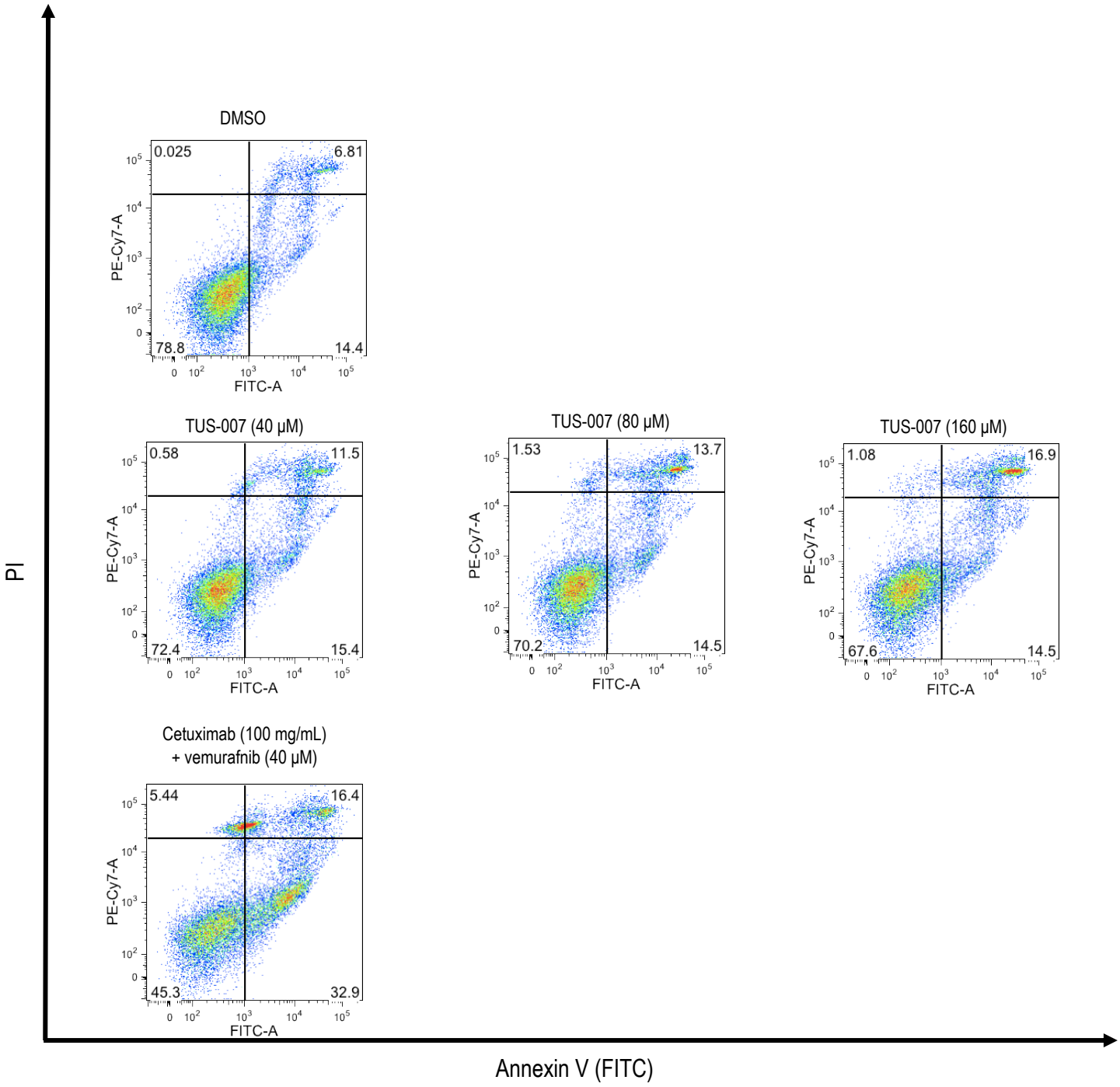

Fig. S6. FACS plots for Annexin V- PI staining of HT29-Luc cells.
HT29-Luc cells were treated with the indicated agents for 48 h, followed by staining with Annexin V-FITC and PI. The typical plots are shown.

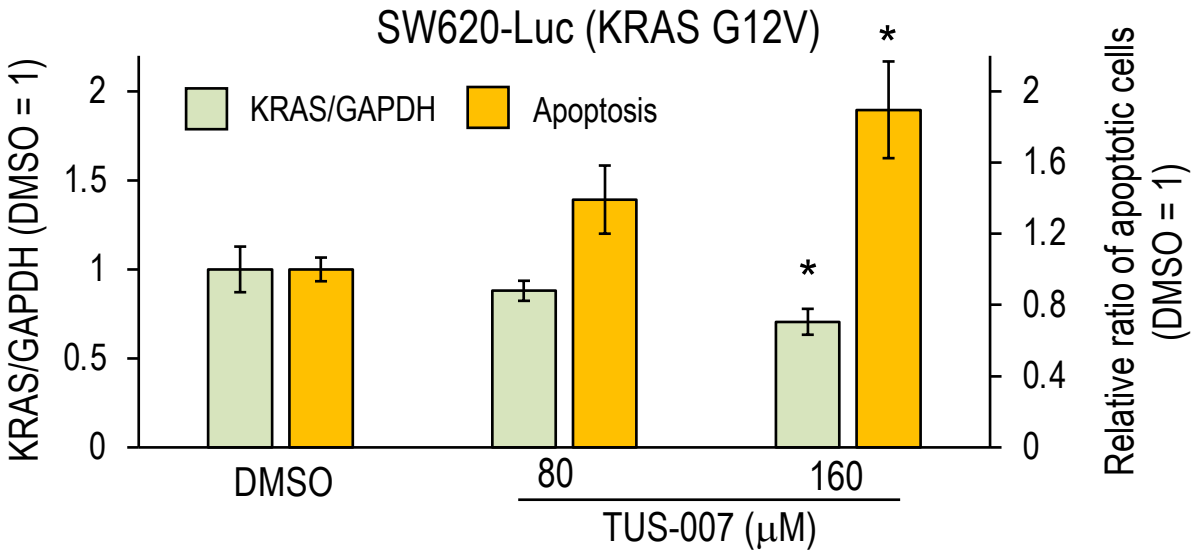

Fig. S7. TUS-007 induced apoptosis only when KRAS degradation was detected in KRAS G12V driven cancer cells. SW620-Luc cell were treated with TUS-007 for 12 h (mean ± SEM; n = 3). The left axis indicates KRAS/GAPDH, and the right axis indicates relative ratio of apoptotic cells. *$P < 0.05$ vs. DMSO. The ratio of KRAS/GAPDH was determined by image analyses of immunoblotting and ration of apoptotic cells were measured using FACS.

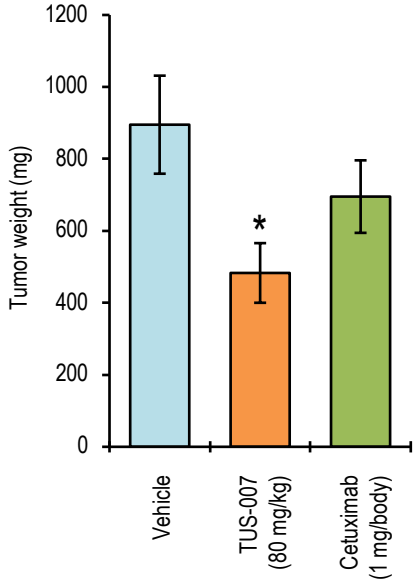

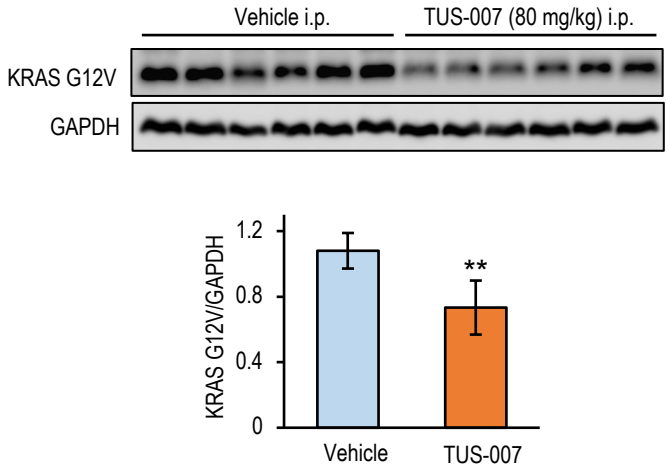

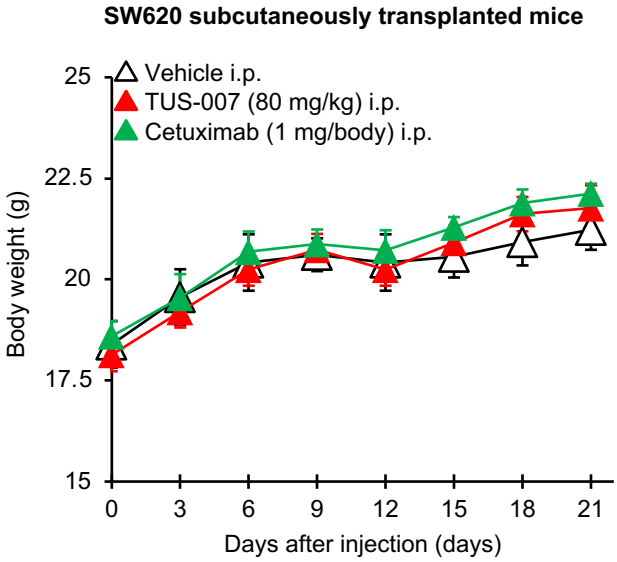

Fig. S8. Effects of TUS-007 on the growth of colon cancer subcutaneous xenografts and toxicity.
a, Comparison of SW620-Luc tumor weight at 21 days after injection (mean ± SEM; n = 6–8). *P < 0.05 vs. vehicle alone. **b,** Immunoblotting of KRAS G12V chemical knockdown in tumors from the same mice used in Fig. 2e (mean ± SEM; n = 6). **P < 0.01 vs. vehicle alone **c,** Body weight changes in mice with SW620-Luc cells transplanted subcutaneously (mean ± SEM; n = 6–8).

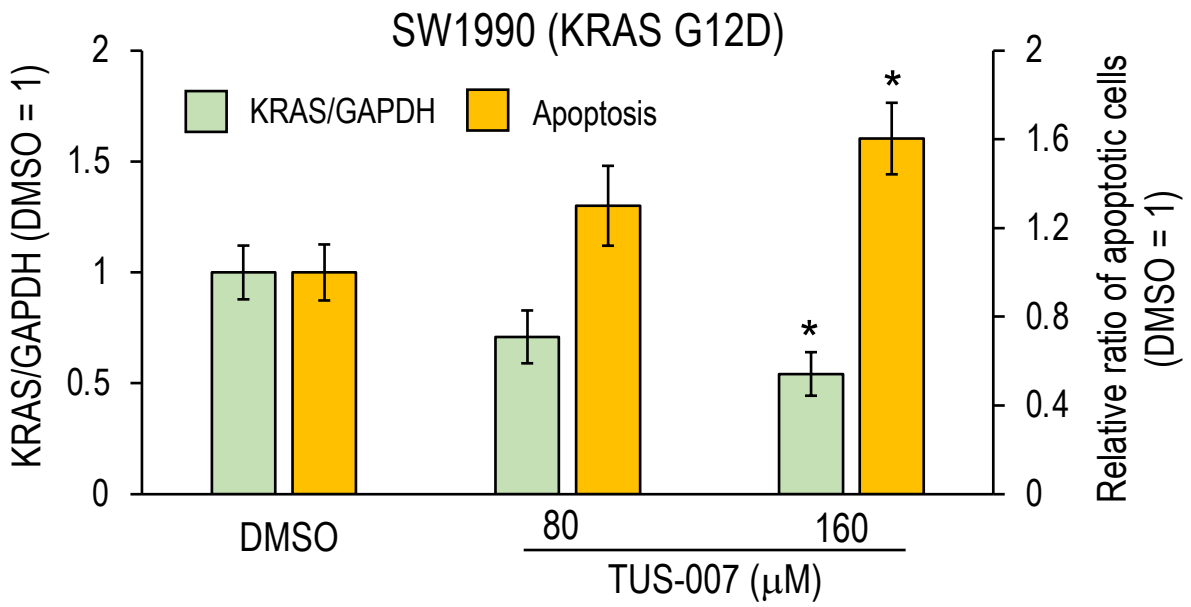

Fig. S9. TUS-007 induced apoptosis only when KRAS degradation was detected in KRAS G12D driven cancer cells. SW1990 cell were treated with TUS-007 for 12 h (mean ± SEM; n = 3).). The left axis indicates KRAS/GAPDH, and the right axis indicates relative ratio of apoptotic cells. *P < 0.05 vs. DMSO. The ratio of KRAS/GAPDH was determined by image analyses of immunoblotting and ration of apoptotic cells were measured using FACS.

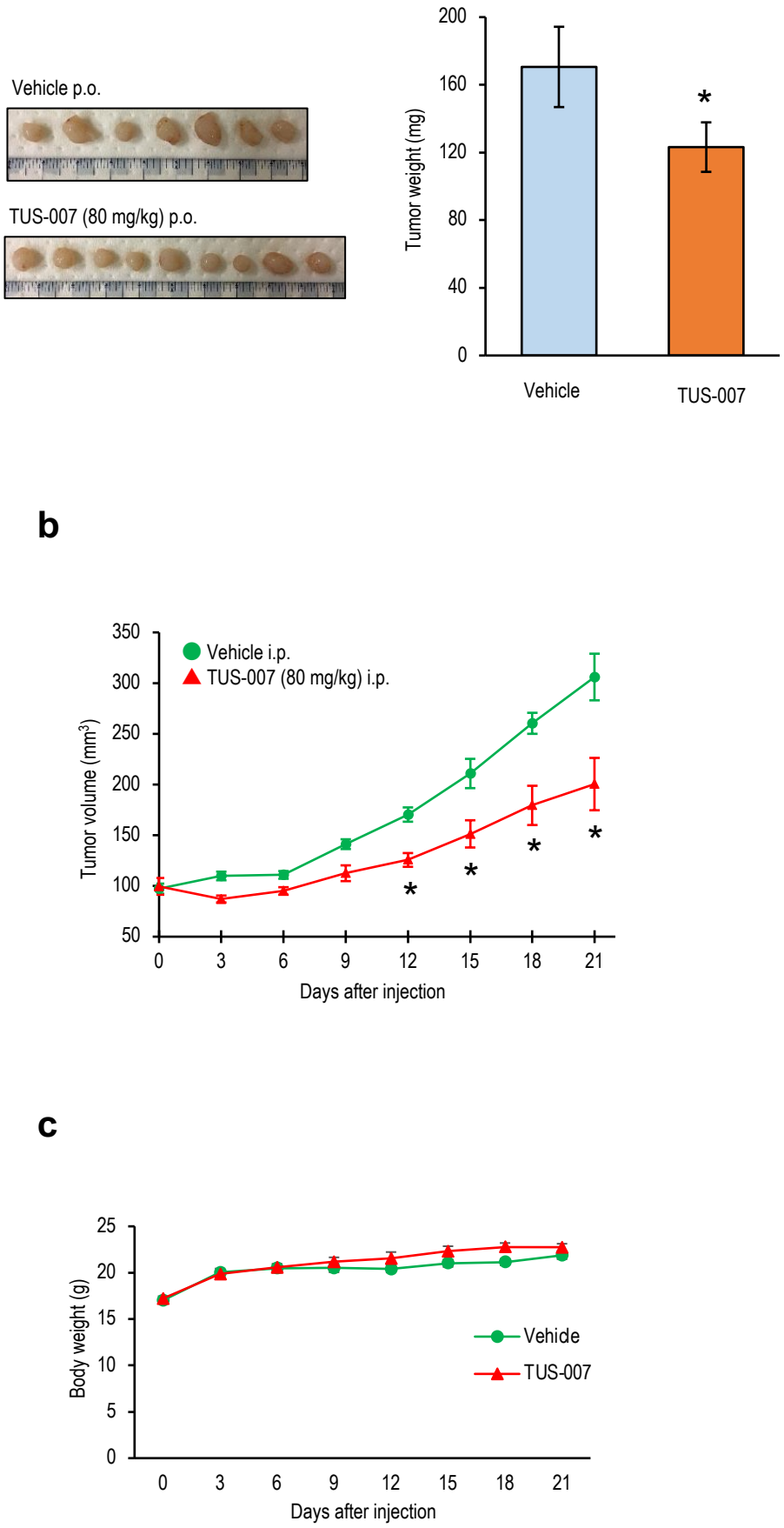

Fig. S10. Effects of TUS-007 on the growth of pancreatic cancer subcutaneous xenografts and toxicity.
a, Tumors of SW1990 cells from the same mice shown and comparison of tumor weight in Fig. 3e at 21 days after p.o. administration (mean ± SEM; n = 6–9). *P < 0.05 vs. vehicle alone. **b,** Tumor volume in mice with SW1990 cells transplanted subcutaneously and treated with i.p. administered TUS-007 or vehicle (mean ± SEM; n = 6–9). The agents were administered every three days. *P < 0.05 vs. vehicle. **c,** Body weight changes in mice with SW1990 cells transplanted subcutaneously (mean ± SEM; n = 6–9).

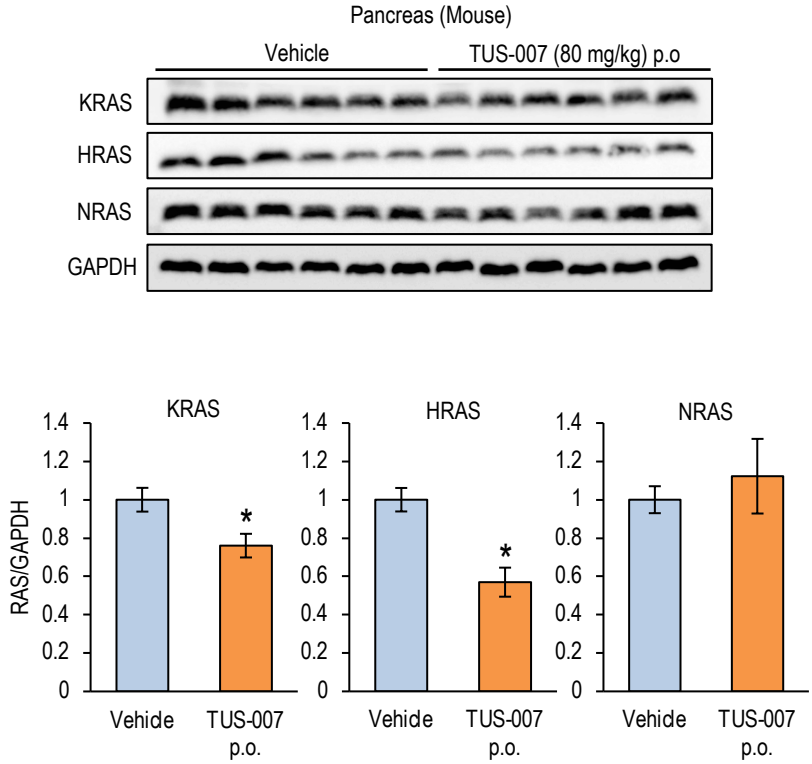

Fig. S11. Effects of oral treatment with TUS-007 on wild type RAS in pancreas.
The immunoblotting analyses of wt RAS proteins in pancreas from the same mice shown in Fig. 3e (mean ± SEM; n = 6–9). *P < 0.05 vs. vehicle alone.

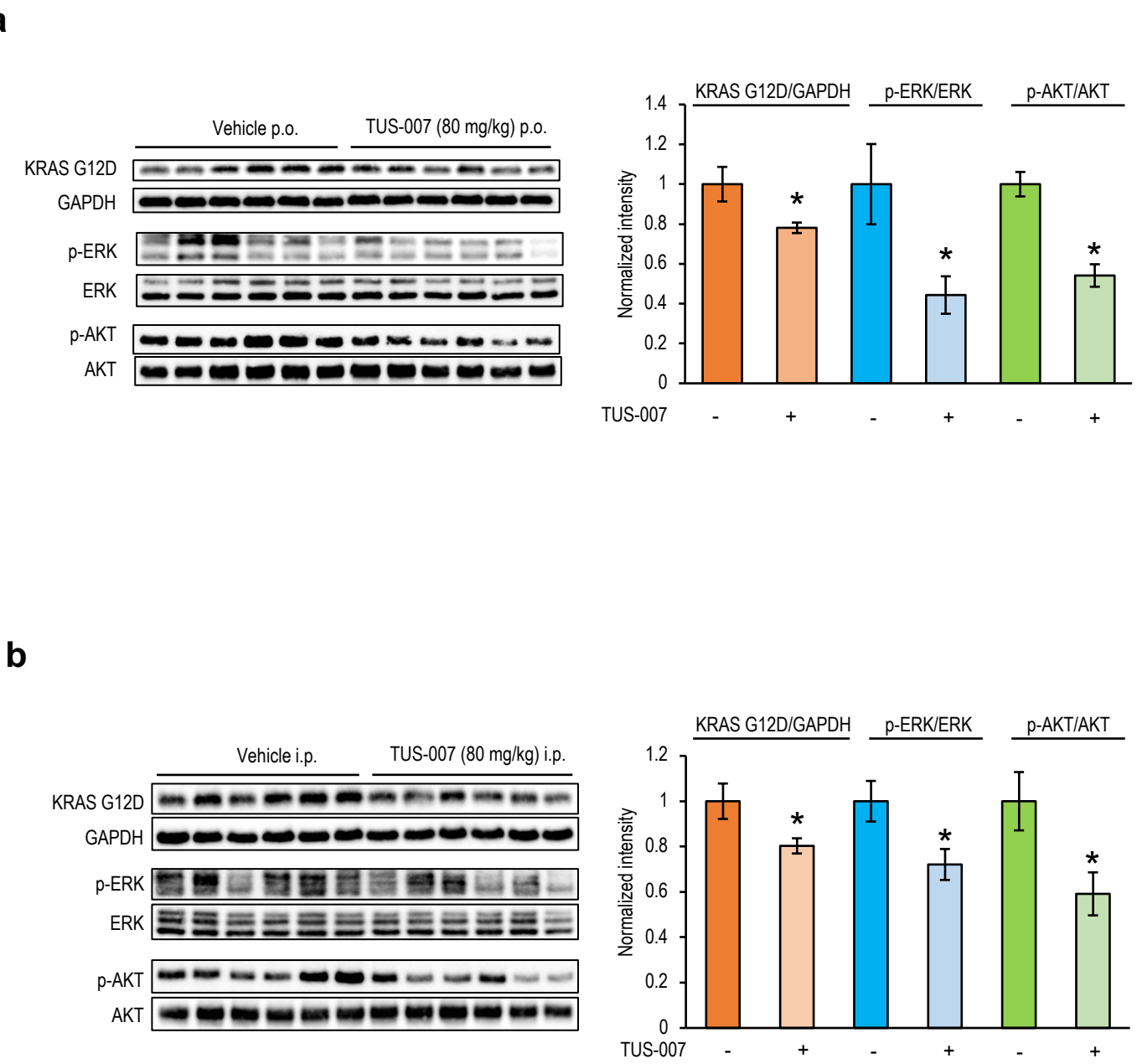

Fig. S12. Effect of of TUS-007 on RAS signaling in pancreatic cancer subcutaneous xenografts. .
Immunoblotting of KRAS and downstream signaling molecules in tumors from the same mice used in Fig 3e (**a**: p.o. treatment) and Supplementary Fig. 11c (**b**: i.p. treatment). The quantitative analysis of the immunoblotting was shown as bar graph, where the KRAS values were normalized to GAPDH, the p-ERK values were normalized to the total ERK, and the p-AKT values were normalized to the total AKT (mean ± SEM; n = 6). *P < 0.05 vs. vehicle.

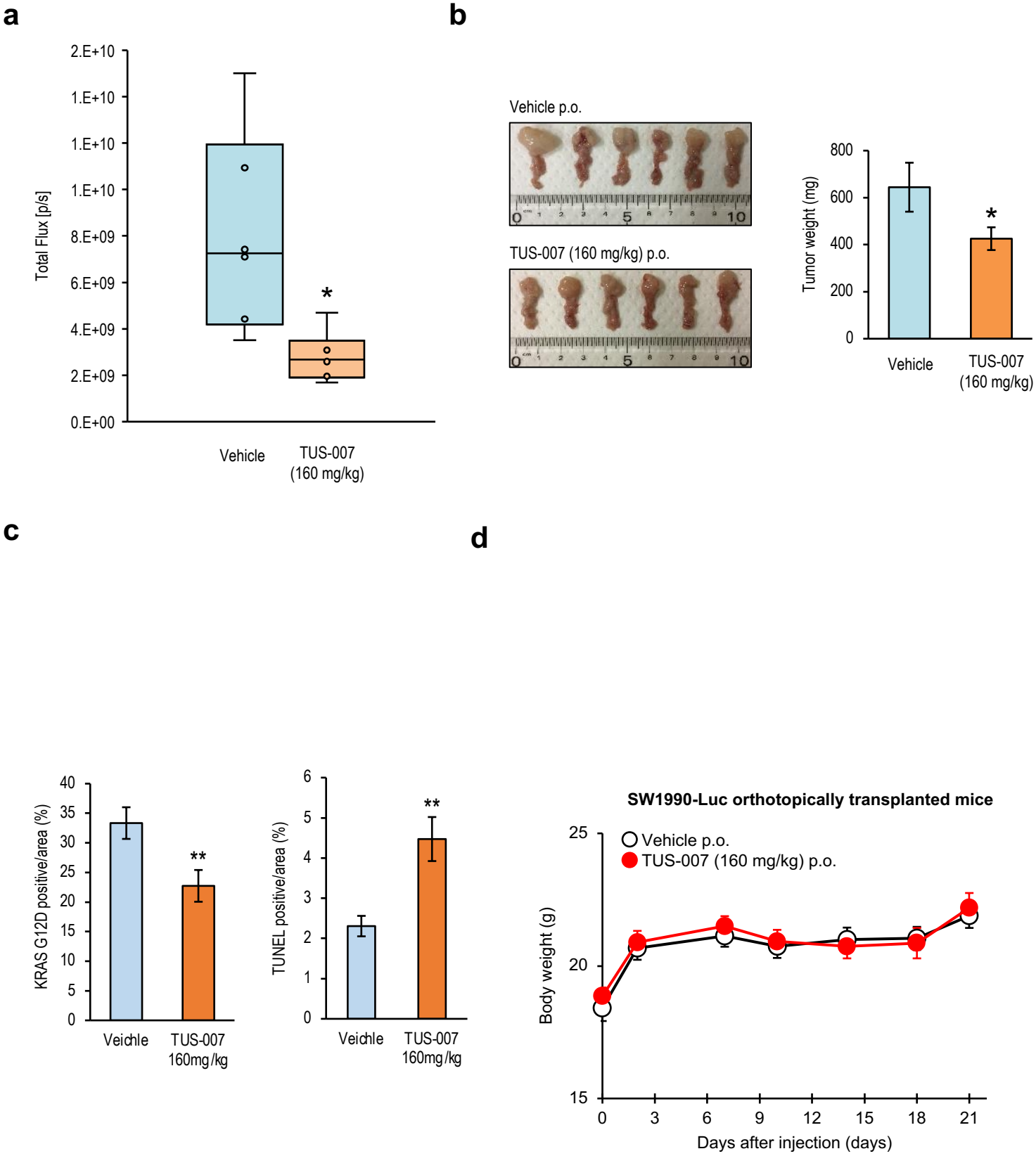

Fig. S13. Effect of TUS-007 on growth of orthotopic pancreatic cancer xenografts expressing mutant KRAS.
a, Tumor growth, as assessed by luciferase signal, in individual mice orthotopically transplanted SW1990-Luc cells treated with TUS-007 (red) or vehicle alone (blue) (mean ± SEM; n = 6). **b,** Pancreases from orthotopic xenograft model mice at day 21 after treatment with TUS-007 (lower-left panel) or the vehicle alone (upper-left panel) and comparison of their weights (right graph) (mean ± SEM; n = 6). *P < 0.05 vs. vehicle alone. **c,** . The quantitative analyses of the KRAS G12D-positive area (left) and TUNEL-positive area (right) in Fig. 4c (mean ± SEM; n = 6). **P < 0.01 vs. vehicle alone. **d**, Body weight changes in mice subjected to orthotopic transplantation of SW1990-Luc cells (mean ± SEM; n = 6).

a

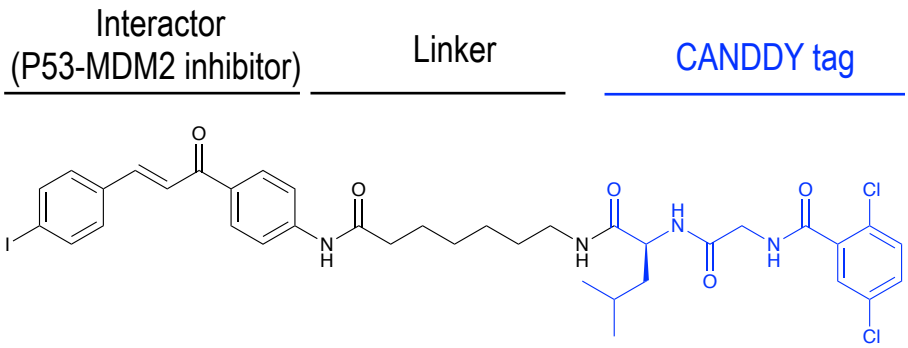

b

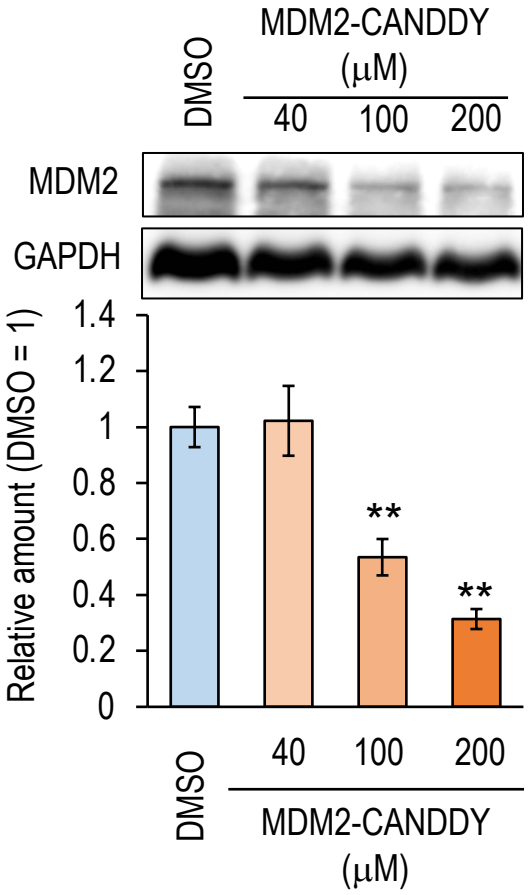

Fig. S14. CANDDY induced degradation of MDM2, a common undruggable target.
a, The structure of MDM2-CANDDY using P53-MDM2 PPI inhibitor, with IC50 value between 6-25 μM. **b,** MDM2-CANDDY degraded MDM2 in the dose dependent manner. The human colon cancer cells HCT-116 were incubated for 48 h with MDM2-CANDDY (mean ± SEM; n = 3). **P < 0.01 vs. DMSO.

Table S1. **The concentration of TUS-007 in pancreas was maintained for 72 h.**
The concentration of TUS-007 in pancreas from healthy wild-type mice i.p. treated with TUS-007 at 80 mg/kg (means ± SEM; n = 5). The samples were obtained at indicated time points after i.p. injection. The concentration of TUS-007 was measured with HPLC.

Hours after i.p	1h	20h	72h
TUS-007 in pancreas (ng/mg)	45.7 ± 20.3	55.0 ± 28.6	61.8 ± 30.0

Table S2. Body weight change in toxicological tests.
TUS-007 did not affected on the body weight changes of mice.

Test Article Dose	Day	1	2	3	4	5	6	8	10	12	15	17	Body weight gain
Control	Mean	30.2	30.3	30.3	30.5	30.1	30.2	30.5	30.8	31.1	31.4	32.1	1.9
0	S.D.	1	1	1	1	1	1	1	1	1	1	1	1
mg/kg	n	5	5	5	5	5	5	5	5	5	5	5	5
TUS-007	Mean	30.2	30.5	30.2	30.3	30.5	30.7	31.0	31.2	31.7	32.1	32.8	2.6
80	S.D.	1	2	1	2	2	2	2	2	2	3	3	1
mg/kg	n	5	5	5	5	5	5	5	5	5	5	5	5

Table S3. **Weight of organs in toxicological tests.**
TUS-007 did not affected on the organ weight of mice.

Test Article Dose		F.B.W.@@ g	Heart mg	Lung mg	Liver g	Spleen mg	Kidney-RL mg
Control	Mean	32.5	147	175	1.81	96	448
0	S.D.	0.9	9	10	0.14	17	34
mg/kg	n	5	5	5	5	5	5
TUS-007	Mean	33.0	157	184	1.78	85	483
80	S.D.	2.6	15	21	0.22	22	68
mg/kg	n	5	5	5	5	5	5

Test Article Dose		Heart mg/100g	Lung mg/100g	Liver g/100g	Spleen mg/100g	Kidney-RL mg/100g
Control	Mean	451	538	5.57	295	1378
0	S.D.	26	19	0.37	45	87
mg/kg	n	5	5	5	5	5
TUS-007	Mean	475	557	5.38	255	1462
80	S.D.	16	37	0.28	52	123
mg/kg	n	5	5	5	5	5

Table S4. Histological observations of organs in toxicological tests.
TUS-007 did not cause histological changes in mice.

Organs	Sex:	M	M
	Group:	Control	TSU-007
	Dose(mg/kg):	0	80
Findings	Number:	5	5
Brain(cerebrum)			
Number examined		5	5
Not remarkable		5	5
Heart			
Number examined		5	5
Not remarkable		5	5
Necrosis/infiltrate		0	0
minimal		0	0
Intestine,rectum			
Number examined		5	5
Not remarkable		5	5
Kidney			
Number examined		5	5
Not remarkable		5	5
Cyst		0	0
minimal		0	0
Liver			
Number examined		5	5
Not remarkable		5	5
Infiltrate,neutrophil		0	0
minimal		0	0
Necrosis,single cell,hepatocyte		0	0
minimal		0	0
Lung(bronchus)			
Number examined		5	5
Not remarkable		5	5
Pancreas			
Number examined		5	5
Not remarkable		5	5
Spleen			
Number examined		5	5
Not remarkable		5	5

M : Male

Table S5. Hematology in toxicological tests.

TUS-007 did not cause hematological changes in mice.

Test Article Dose		RBC 10E4/µL	HGB g/dL	HCT %	MCV fL	MCH pg	MCHC g/dL	Retic 10E9/L	PLT 10E4/µL
Control	Mean	881	13.5	47.2	53.5	15.3	28.7	241.4	113.2
0	S.D.	59	0.7	2.9	0.9	0.5	0.8	26.9	7.0
mg/kg	n	5	5	5	5	5	5	5	5
TUS-007	Mean	876	13.3	46.4	53.1	15.2	28.6	281.2	120.8
80	S.D.	53	0.4	1.4	2.7	0.8	0.4	70.7	3.0
mg/kg	n	5	5	5	5	5	5	5	5

Test Article Dose		WBC 10E2/µL	LYMP 10E2/µL	NEUT 10E2/µL	EOS 10E2/µL	BASO 10E2/µL	MONO 10E2/µL	LUC 10E2/µL
Control	Mean	42.5	32.3	7.8	1.4	0.0	0.9	0.0
0	S.D.	6.2	3.9	3.2	0.6	0.1	0.3	0.1
mg/kg	n	5	5	5	5	5	5	5
TUS-007	Mean	37.5	28.3	6.8	1.1	0.0	1.2	0.1
80	S.D.	14.2	12.0	3.0	0.4	0.1	0.7	0.1
mg/kg	n	5	5	5	5	5	5	5

Table S6. Biochemical examinations in toxicological tests.
TUS-007 did not cause biochemical changes in mice.

Test Article Dose		AST IU/L	ALT IU/L	LDH IU/L	ALP IU/L	TG mg/dL	GLU mg/dL	BUN mg/dL	CRNN mg/dL	TP g/dL	ALB g/dL	ALB g/dL
Control	Mean	40	31	207	256	104	230	19	0.22	4.7	3.2	0.2594
0	S.D.	6	6	65	68	41	17	3	0.04	0.1	0.1	0.1062
mg/kg	n	5	5	5	5	5	5	5	5	5	5	5
TUS-007	Mean	35	24	151	265	85	226	19	0.19	4.9	3.2	0.2308
80	S.D.	3	2	33	28	31	31	2	0.04	0.1	0.2	0.0763
mg/kg	n	5	5	5	5	5	5	5	5	5	5	5